EFFECTS OF AIRFRAME CONFIGURATION ON LOW-FREQUENCY ANTENNA CHARACTERISTICS

CHARLES MINOR HOBLITZELL

1953

M-45

EFFECTS OF AIRFRAME CONFIGURATION ON LOW-FREQUENCY ANTENNA CHARACTERISTICS

C. M. Hoblitzell

EFFECTS OF AIRFRAME CONFIGURATION ON LOW-FREQUENCY ANTENNA CHARACTERISTICS

by

Charles Minor Hoblitzell
Lieutenant, United States Navy

Submitted in partial fulfillment
of the requirements
for the degree of

MASTER OF SCIENCE

IN

ENGINEERING ELECTRONICS

United States Naval Postgraduate School
Monterey, California
1953

This work is accepted as fulfilling

the thesis requirements for the degree of

MASTER OF SCIENCE

IN

ENGINEERING ELECTRONICS

from the

PREFACE

This work is an application of a technique developed by Stanford Research Institute for determining the characteristics of low-frequency dipole-type antennas by electrostatic measurements. Specifically it concerns the variation in the radiation patterns of low-frequency aircraft antennas due to the airframe configuration and the location on a particular airframe. The different configurations are simulated by adding wing, tail surfaces and nacelles in varying combinations to a slender prolate spheroid. The experimental results include a comparison of mock-up measurements with actual aircraft model measurements.

The writer wishes to acknowledge the contributions made to this work by the members of the Aircraft Radiation Systems Laboratory at Stanford Research Institute. Particular thanks are due to Dr. J. T. Bolljahn and Mr. R. F. Reese for their many discussions and suggestions on both the practical and the theoretical aspects concerned.

This work is an application of a technique developed by Stanford Research Institute for determining the characteristics of low-frequency dipole-type antennas by electrostatic measurements. Specifically it concerns the variation in the radiation patterns of low-frequency aircraft antennas due to the airframe configuration and the location on a particular airframe. The different configurations are simulated by adding wing, tail surfaces and nacelles in varying combinations to a slender prolate spheroid. The experimental results include a comparison of mock-up measurements with actual aircraft model measurements.

The writer wishes to acknowledge the contributions made to this work by the members of the Aircraft Radiation Systems Laboratory at Stanford Research Institute. Particular thanks are due to Dr. J. T. Bolljahn and Mr. T. P. Tesco for their many discussions and suggestions on both the practical and the theoretical aspects concerned.

TABLE OF CONTENTS

TABLE OF CONTENTS

LIST OF ILLUSTRATIONS

LIST OF ILLUSTRATIONS (Cont'd)

CHAPTER I

INTRODUCTION

The measurement of low frequency dipole-type antenna characteristic using electrostatic techniques is a recent development in antenna research. The analogue technique has been used by Bolljahn [1] and Reese [5] to provide design information for a number of specific aircraft antenna installations. The use of this technique is not limited solely to aircraft, but may be applied to any antenna installation in which the dimensions of both the antenna and the body on which it is mounted are small relative to a wavelength at the operating frequency. The information obtained from electrostatic measurements is the effect of the conducting body on the sensitivity and the radiation pattern of any dipole-type antenna. This knowledge may be applied to an antenna of specific size and shape in order to evaluate its characteristics and compare them with the desired specifications.

Since the antennas to which this technique is applicable are small, the radiation pattern is that of a simple dipole. The only effect of the conducting body is to vary the orientation of the pattern for various locations on the body. The combination of the antenna and the conducting body form what may be termed as equivalent dipole. The angle by which the axis of this equivalent dipole departs from a vertical orientation is of particular interest in the placement of ADF sense antennas on aircraft. This angle of tilt must be small or erroneous navigational information will be supplied by the ADF system. The

CHAPTER I

curvature of the conducting body at any point causes an intensification of the field normal to the surface at that point. This results in an increase in the sensitivity of an antenna mounted at that location when compared with its sensitivity to an incident wave while mounted on flat ground plane. The ratio of the field normal to the surface of the conducting body to the uniform field in which the body is immersed is a direct measure of this increase in sensitivity. This ratio is called the curvature factor and is a function of the aircraft configuration as well as the location on any specific airframe.

The ability to predict more accurately the radiation characteristics of an antenna on a particular aircraft would be extremely useful in preliminary discussions and planning prior to making measurements on the actual model. This investigation is intended to make such predictions possible by observing the effects of the various major airframe components as they are added to the fuselage or combined in various ways to simulate existing aircraft configurations.

The initial step in the investigation is a discussion of the theory of small dipole-type antennas and a justification of the quasi-static approach to the problem. The quasi-static solutions for simple antenna configurations are used to define a new sensitivity parameter for antennas. An experimental technique suggested by the theoretical discussion is outlined and the facilities required to implement this technique are discussed. The experimental results include the simulated aircraft measurements and measurements of actual aircraft. The use of the data obtained from the simulated configurations in predicting the

aircraft characteristics is demonstrated. These predictions are compared with the measurements obtained from actual models and the probable reasons for discrepancies between the predicted and the measured results are indicated. The final discussion concerns the refinements in prediction which are possible by correlating the results of this study with past and future data obtained from actual models.

CHAPTER II

THEORY OF SMALL DIPOLE-TYPE ANTENNAS

The properties of small antennas of the dipole-type have been reported in an extensive study by J. T. Bolljahn [2] of the Stanford Research Institute. This section is a summary of the portion of the above report pertinent to this investigation. It contains the development and justification of the electrostatic solution for small antenna characteristics and the theoretical definition of the qantities which may be determined using this technique. The figures and curves referred to in the discussion have been taken from the above report with the kind permission of Stanford Research Institute and Dr. Bolljahn.

1. The Equivalent Generator Circuit

The antennas under investigation in this study are those for which both the antenna size and the dimensions of airframe on which it is mounted are small relative to the operating wave length. This situation is encountered in sense antennas for aircraft ADF systems and also for LORAN antennas on aircraft. Figure 1 shows the equivalent generator circuit commonly associated with this type antenna. The source impedance is equal to the driving point impedance of the antenna and the generated voltage is proportional to the amplitude of the incident wave.

For an antenna with a matched load the proportionality existing between the equivalent open-circuit generator voltage and the incident wave amplitude is given in terms of the antenna properties by

$$\frac{V_{oc}}{E} = 2\sqrt{\frac{R_a A}{\eta}} \qquad (1)$$

where

V_{oc} = Equivalent open-circuit generator voltage (Volts)

E = Amplitude of the incident electric field (Volts/Meter)

R_a = Resistance component of antenna impedance (Ohms)

A = Receiving crossection of antenna (Meters^2)

η = 120 Ohms

The factor A contains the functional dependence of the ratio on the antenna orientation relative to the direction of propagation and the polarization of the incident wave. The maximum value of the ratio is designated by the term "effective length", symbolically abbreviated l_e. Thus

$$l_e = \frac{V_{oc\,max}}{E} = 2\sqrt{\frac{R_a A_{max}}{\eta}} \qquad (2)$$

For linear antennas the value of l_e is simply related to the antenna dimensions; but for other types, such as a cavity antenna, there exists no such simple relation. The use of the alternative form of equivalent generator circuit shown in Figure 2 makes it possible to define a sensitivity parameter for any small dipole-type antenna. This circuit consists of an infinite impedance current generator shunted by an admittance equal to the antenna driving-point admittance. The magnitude of the generator current is equal to the current which would flow through the antenna terminals if these were short circuited. The use of this form of equivalent generator makes calculation of the generator current particularly simple for small flush-mounted antennas.

$$\frac{\partial}{\partial x}$$

Suppose a uniform static electric field is impressed such that it strikes a conducting sheet normally as shown in Figure 3. If the terminals of the flush antenna are short circuited, and if the gap width is small relative to the size of the opening in the sheet, the electric field will be uniform except for small perturbations in the vicinity of the gap. The charge induced on the antenna by the impressed field is given by

$$q = \varepsilon_o E_o S \tag{3}$$

where

q = Induced charge (Coulombs)

ε_o = Dielectric constant of free space (Farads/Meter)

E_o = Magnitude of incident static field (Volts/Meter)

S = Area enclosed by slot (Meters^2)

If the impressed field is now allowed to vary slowly in a periodic fashion such that

$$E = E_o e^{j\omega t} \tag{4}$$

then the current through the shorted antenna terminals is given by

$$I_s = j\omega q = j\omega \varepsilon_o E S \tag{5}$$

where

I_s = Equivalent generator current (Ampere)

ω = Angular frequency (Radians/Second)

The condition that the frequency be low corresponds to the assumed condition that the dimensions of the antenna system be small relative to

the wave length. The equivalent generator currents for other forms of small antennas may be calculated in the same manner.

If the induced charge on a small antenna of arbitrary form can be determined, equation 3 may be used to define a new sensitivity parameter a_e. This parameter can be termed the "equivalent area" of the antenna in question. In terms of the induced charge and the impressed static field

$$a_e = \frac{q}{\varepsilon_o E_o} \tag{6}$$

For a flush antenna, this reduces to the area S enclosed by the slot. This parameter, like l_e, is function of the particular antenna configuration. The equation for the equivalent generator current may be written for the general case as

$$I_s = j\omega \varepsilon_o E a_e \tag{7}$$

Since the two equivalent generator circuits apply equally well to the same antenna, there must exist a relationship between the sensitivity parameters l_e and a_e. An expression for the equivalent generator current may be obtained by dividing the open-circuit voltage V_o by the antenna impedance. For all very small antennas of the dipole type the resistance component of the impedance is sufficiently small so that the equivalent generator impedance may be represented by a pure capacitance C_a. Equating this result to the expression for the current given by equation 7 results, upon simplification, in

$$a_e = \frac{C_a l_e}{\varepsilon_o} \tag{8}$$

The equivalent area is thus proportional to the product of the antenna capacitance and the effective length.

2. Ground Plane Effects

The extension of the preceding discussion to protruding antennas can best be accomplished by considering the conducting body on which the antenna is mounted as a ground plane "against" which the radiator is driven. This requires separation of antenna and ground plane effects.

For a small flush antenna located on the surface of a conducting body the determination of the induced charge due to an impressed static field permits evaluation of a_e and the equivalent generator current. If the dimensions of a small protruding antenna are small relative to the radius of curvature on which it is mounted, the ratio of induced charges on a flush antenna and a protruding antenna should be very nearly the same as the corresponding ratio when both antennas are located on a plane conductor. The arguments applied above to the calculation of induced charge on flush antennas may thus be extended to protruding antennas.

The effect of the conducting body on the system sensitivity is apparent if equation 6 is written in the form

$$a_e = \frac{q}{\varepsilon_o E_n} \cdot \frac{E_n}{E_o} \tag{9}$$

where E_n is the electric field normal to the conducting surface due to the impressed field E_o, in the absence of the antenna. The factor

$q/\varepsilon_o E_n$ is taken as the sensitivity parameter for the antenna on an infinite plane conductor and the factor E_n/E_o represents the effect of the conducting body.

If the conducting body is small relative to a wavelength, electrostatic solutions may be used to determine the ratio E_n/E_o. According to Smythe [6] this ratio attains a maximum value of 2 for a long cylindrical conductor and 3 for a sphere as illustrated in Figure 4. The sensitivity parameter of a small antenna mounted on such conducting surfaces is increased by this amount over its value on a plane conductor.

A geometrical form of particular interest is the prolate spheroid because of its resemblance to an aircraft fuselage. Spheroidal solutions may be used to calculate the factor E_n/E_o for spheroids having various major-to-minor-axis ratios. The results are shown in Figures 5 and 6 for the impressed field respectively parallel and perpendicular to the major axis of the spheroid. For polarization parallel to the major axis the values of E_n/E_o are large near the end of the conductor. This demonstrates the advantage of locating the antenna near an extremity of a conducting body (as is done with wing-cap and tail-cap antennas) provided that an undesirable radiation pattern does not result from such a location. For polarization perpendicular to the major axis the factor E_n/E_o approaches 2 for most of the length of relatively thin spheroids. The limiting case is an infinitely long cylinder for which the value is exactly 2.

The case of arbitrary incidence of the impressed field relative to the major axis of the spheroid may be treated as a combination

$Q/\varepsilon_0 E^m$ is taken as the sensitivity parameter for the antenna on an infinite plane conductor and the factor E^m/E^m_0 represents the effect of the conducting body.

If the conducting body is small relative to a wavelength, electrostatic solutions may be used to determine the ratio E^m/E^m_0. According to Smythe [6] this ratio attains a maximum value of 2 for a long cylindrical conductor and 3 for a sphere as illustrated in Figure 4. The sensitivity parameter of a small antenna mounted on such conducting surfaces is increased by this amount over its value on a plane conductor.

A geometrical form of particular interest is the prolate spheroid because of its resemblance to an aircraft fuselage. Spheroidal solutions may be used to calculate the factor E^m/E^m_0 for spheroids having various major-to-minor-axis ratios. The results are shown in Figures 5 and 6 for the impressed field respectively parallel and perpendicular to the major axis of the spheroid. For polarization parallel to the major axis the values of E^m/E^m_0 are large near the end of the conductor. This demonstrates the advantage of locating the antenna near an extremity of a conducting body (as is done with wing-cap and tail-cap antennas) provided that an undesirable radiation pattern does not result from such a location. For polarization perpendicular to the major axis the factor E^m/E^m_0 approaches 2 for most of the length of a relatively thin spheroid. The limiting case is an infinitely long cylinder for which the value is exactly 2.

The role of radiating impedance of the impressed field and its relation to the major axis of an spheroid may be noted [ ] as a useful

of the above cases. Superimposing the results for parallel and perpendicular polarization with proper amplitudes results in a radiation pattern which may be shown to be a simple dipole pattern for any location on the spheroid. The orientation of the pattern depends on the location on the spheroid and the major-to-minor-axis ratio of the spheroid. Figure 7 shows the angle between the radiation null and the major axis of the spheroid as a function of the spheroid parameters and the antenna location.

of the above cases. Superimposing the results for parallel and perpendicular polarization with proper amplitudes results in a radiation pattern which may be shown to be a simple dipole pattern for any location on the spheroid. The orientation of the pattern depends on the location on the spheroid and the major-to-minor-axis ratio of the spheroid. Figure 7 shows the angle between the radiation null and the major axis of the spheroid as a function of the spheroid parameters and the antenna location.

CHAPTER III

EXPERIMENTAL MEASUREMENT TECHNIQUE

The discussion in Chapter II is concerned with analytical solutions for the sensitivity parameters of antennas which are of relatively simple configuration. The general development suggests an experimental approach which may be used in determining the characteristics of more complex systems.

Suppose that a conducting model of an aircraft is immersed in a uniform electrostatic field of known intensity. If the charge induced on a small probing antenna mounted on the model can be determined, the sensitivity parameter for that particular location may be calculated. The probing antenna must be small compared to the dimensions of the model at the particular location to minimize the perturbations of the field due to the presence of the antenna. The orientation of the low frequency radiation pattern may be determined by repeating the measurement of charge for various angles of incidence of the impressed static field relative to the aircraft. Typical patterns are shown in figure 8.

Orientation of the aircraft model with the longitudinal axis of the fuselage perpendicular to the impressed field duplicates a condition normally encountered in low frequency aircraft radiation systems. This is the equivalent of a vertically polarized plane wave approaching the aircraft from any azimuth angle. The increase in sensitivity of any small antenna when located at a given point on the airframe can be determined for this case if the ratio E_n/E_o can be evaluated. The

CHAPTER III

EXPERIMENTAL MEASUREMENT TECHNIQUE

The discussion in Chapter II is concerned with analytical solutions for the sensitivity parameters of antennas which are of relatively simple configuration. The general development suggests an experimental approach which may be used in determining the characteristics of more complex systems.

Suppose that a conducting model of an aircraft is immersed in a uniform electrostatic field of known intensity. If the charge induced on a small probing antenna mounted on the model can be determined, the sensitivity parameter for that particular location may be calculated. The probing antenna must be small compared to the dimensions of the model at the particular location to minimize the perturbations of the field due to the presence of the antenna. The orientation of the low frequency radiation pattern may be determined by repeating the measurement of charge for various angles of incidence of the impressed static field relative to the aircraft. Typical patterns are shown in Figure .

Orientation of the aircraft model with the longitudinal axis of the fuselage perpendicular to the impressed field implies a condition normally encountered in low frequency aircraft radiation systems. This is the equivalent of a vertically polarized plane wave approaching the aircraft from any azimuth angle. The increase in sensitivity of any small antenna when located at a given point on the fuselage can be determined for this case if the radio E_{θ}/E_{ϕ} can be [illegible]. The

ratio E_n/E_o is called the curvature factor (normally for the vertically polarized case, although it can be specified for any angle of incidence of the field.) The curvature factor for a given airframe location may be determined by measuring the induced charge on a small antenna of any convenient shape when it is mounted first on the model aircraft and then on the ground plane.

In actual practice the ratio E_n/E_o for any particular location on the model is more accurately determined from the charge pattern obtained by measurements at various orientations relative to the static field. It may be shown that the charge induced on the model for vertical polarization of the incident wave is equal to the maximum charge at that location multiplied by the cosine of the tilt angle. Since the charge pattern varies with the model orientation in the same manner as the radiation pattern of a dipole, a polar plot of the charge variation should result in two tangent circles of equal diameter. The experimentally determined values seldom produce exact circles when plotted, due to errors in the measurement technique. The values of maximum charge and tilt angle are determined from the circles best approximated by the experimental values. Determination of E_n/E_o in this manner makes use of all the measurements at a particular test location rather than a single measurement.

The sensitivity parameter for a particular antenna may be determined by modeling the antenna to a larger scale and making accurate measurements of the charge induced when this model is mounted on a ground plane. The increased size makes it possible to reproduce details of the antenna

ratio E_v/E_0 to obtain the a posteriori factor (correctly for the vertically polarized case, although it can be specified for any angle of incidence of the field.) The corrective factor for a given elevation may be determined by measuring the induced charge on a small antenna of any convenient shape when it is mounted first on the model simulated ocean and then on the ground plane.

In actual practice the ratio E_v/E_0 for any particular location on the model is more accurately determined from the charge pattern obtained by measurements at various orientations relative to the static field.

It may be shown that the charge induced on the model for vertical polarization of the field without warp is equal to the maximum charge at that location multiplied by the cosine of the tilt angle. Since the charge pattern varies with the model orientation in the same manner as the radiation pattern of a dipole, a polar plot of the charge variation should result in two tangent circles of equal diameter. The experimentally determined values will for practical purposes exactly duplicate those obtained by measurement techniques. The values of E_v/E_0 in the region of all the measurements at a particular location yield a single measurement.

The [illegible] parameter for a particular [illegible] to a larger scale and [illegible] the [illegible] factors. Where this model is [illegible]. The

construction which affect its characteristics, but which are not necessary for the determination of the curvature factor. The equivalent area of the scale model thus determined may be converted to the value for the full-scale antenna from the knowledge that for two geometrically similar antennas the ratio of the equivalent areas is the square of the linear scale factor, with the larger antenna having the larger equivalent area. The sensitivity parameter for the full-scale antenna mounted on the aircraft may be calculated by multiplying the ground plane value thus determined by the curvature factor appropriate to the desired location.

This investigation is primarily concerned with the effects of the airframe configuration on the characteristics of small antennas. As shown in Chapter II, the sensitivity parameter is proportional to the product $C_a l_e$. For a particular antenna the determination of the full-scale equivalent area together with the precise measurement of C_a permits the separation of this product into its component values C_a and l_e. Since these parameters are a function of the antenna design and not of the airframe configuration, the measurement of C_a is not required in this study.

configuration which affect its characteristics, but which are not necessary for the determination of the curvature factor. The equivalent area of the scale model thus determined may be converted to the value for the full-scale antenna from the knowledge that for two geometrically similar antennas the ratio of the equivalent areas is the square of the linear scale factor, with the larger antenna having the larger equivalent area. The sensitivity parameter for the full-scale antenna mounted on the aircraft may be calculated by multiplying the ground gain value thus determined by the curvature factor appropriate to the design location.

This investigation is primarily concerned with the effects of the airframe configuration on the characteristics of small antennas. As shown in Chapter II, the sensitivity parameter is proportional to the product $G_g l_e$. For a particular antenna the determination of the full-scale equivalent area together with the precise measurement of G_g permits the separation of this product into its component values G_g and l_e. Since these parameters are a function of the antenna design and not of the airframe configuration, the measurement of G_g is not required in this study.

CHAPTER IV

MEASUREMENT FACILITIES

Measurements of the equivalent dipole tilt angle (orientation of the radiation null) and the curvature factor were obtained in the electrostatic cage. Figure 9 is a sketch of the cage showing the conducting end plates with surrounding guard-ring wires and resistance voltage divider to minimize fringing of the field.

The model to be measured is mounted on an insulated shaft with the fuselage centerline perpendicular to the shaft. Provisions must be made for mounting the model on either the top or the bottom of the fuselage to place the shaft as far as possible from the points at which measurements are to be taken. The insulated shaft passes through the electrostatic cage at the center parallel to the conducting end plates. The ends of the shaft are mounted in bearings permitting orientation of the model at any desired angle relative to the incident field.

A rigid probe was developed for removing the charged probing antenna from the cage. The antenna is fixed in a short section of Teflon threaded on a four inch length of one-eighth inch diameter Nylon rod. This provides the necessary stiffness with the minimum perturbation of the field in the vicinity of the antenna. It also provides excellent insulation of the charged antenna, limiting the leakage of the probing system to orders of magnitude smaller than the measurement capabilities of the electrometer. The Nylon rod is attached to a Fiberglas rod of larger diameter approximately three feet in length. This allows positioning of the antenna in a small location hole at the

CHAPTER IV

MEASUREMENT FACILITIES

Measurements of the equivalent dipole tilt angle (orientation of the radiation null) and the curvature factor were obtained in the electrostatic cage. Figure 9 is a sketch of the cage showing the construction and plates with surrounding guard-ring wires and resistance voltage divider to minimize distortion of the field.

The model to be measured is mounted on an insulated shaft within the fuselage centerline perpendicular to the shaft. Provisions must be made for mounting the model on either the top or the bottom of the fuselage to place the shaft as far as possible from the points at which measurements are to be taken. The insulated shaft passes through the electrostatic cage at the center parallel to the conducting end plates. The ends of the shaft are mounted in bearings permitting orientation of the model at any desired angle relative to the incident field.

A right probe was developed for receiving the energy probing antenna from the cage. The antenna is fixed in a short section of Teflon threaded on a four inch length of one-eighth inch diameter lucite rod. This provides the necessary stiffness with the minimum perturbation of the field in the vicinity of the antenna. It also provides excellent insulation of the charged antenna, limiting the leakage of the probing system to orders of magnitude smaller than the measurement capabilities of the electrometer. The lucite rod is soldered to a fifteen foot length of Lafayette microphone cable. This cable is wrapped with aluminum foil for the length of the antenna in a small loop at the

desired fuselage station from outside the electrostatic cage.

The d-c field is impressed with the antenna in place on the model causing a separation of charge. The antenna is removed with the induced charge while the field is still present. Although removal of the antenna disturbs the charge distribution both on the aircraft and the antenna, the total quantity of charge removed remains the same. The field is then removed and the charged antenna placed inside a brass cup at the input of a sensitive electrometer. This brass cup, which is shielded by another coaxial grounded cylinder, acts as a Faraday "ice-pail" since its capacitance to ground is independent of the size or shape of the charged body placed in it. The voltage on this capacitor therefore depends only on the charge it has received. Typical values of measured charge for this study ranged from 35 to 445 micro-micro-coulombs at the radiation pattern maximum. The experiment was conducted with a d-c potential of 17.5 kilovolts impressed across the conducting end plates of the electrostatic cage. This corresponds to a field intensity of approximately 11,000 volts per meter.

Figure 10 is photograph of the facilities described above under actual measurement conditions.

The prolate spheroid and the different wing and tail assemblies with which various aircraft configurations are simulated are shown in Figure 11. In order to dimension the prolate spheroid properly a survey was made of a number of representative aircraft. The average fuselage length-to-diameter ratio of 9.08 for the various aircraft led to the choice of a 9:1 major-to-minor axis ratio for the spheroid. The length of the

spheroid was chosen as 27 inches. Bolljahn [3] has shown that with a spacing of 60 inches between the end plates of the electrostatic cage, this length is an optimum size for obtaining measurable charge without producing undesirable perturbations of the field due to images.

The principal dimensions of the other airframe components were similarly related to the fuselage length and the ratios averaged to determine the sizes and shapes of the simulating components. Figures 12, 13, and 14 are photographs of three configurations illustrating the flexibility of the mock-up in simulating complete airframes.

CHAPTER V

EXPERIMENTAL RESULTS

The discussion which follows is based on the results of an investigation conducted by the writer [4] for Stanford Research Institute during the ten-week industrial experience tour of duty.

1. Measurements on Prolate Spheroid Mock-Up

The equivalent dipole tilt angle and the curvature factor may be calculated for different positions on the prolate spheroid from the field equations as discussed in Chapter II. This was done for the prolate spheroid used in this study as a check on the calibration of the entire system. Figure 15 is a plot of the calculated values with the experimentally determined values superimposed. The close agreement of experimental and calculated values is indicative of the accuracy of measurement obtainable with this system.

A low-wing configuration was chosen to illustrate the incremental effects of the various airframe components as they are added to the prolate spheroid in logical succession. The results are shown for top centerline stations in Figure 16 and bottom centerline stations in Figure 17. In the former case the tilt angle curve shifts forward as the wing is added and backward with the addition of the horizontal stabilizer. The only other change is the decrease in tilt angle at stations near the tail with the addition of the vertical fin. The wing alone raises the curvature factor along the top of the fuselage, but the major effect is the rapid decrease in curvature factor near the tail when the vertical fin is added.

CHAPTER V

EXPERIMENTAL RESULTS

For the stations along the bottom centerline of the fuselage the addition of the wing has little effect on the tilt angle forward of the wing centerline. There is an initial increase in tilt angle aft of the wing, followed by a continual decrease as succeeding components are added. An increase in curvature factor due to the addition of the horizontal stabilizer and the vertical fin accompanies the decrease in tilt angle at stations near the tail and makes the shielding effect of the wing more pronounced. The addition of nacelles further increases the shielding effect forward of the wing along the bottom of the fuselage but has negligible effect on the top stations.

As the position of a straight (0-degree sweepback) wing alone is varied from top to bottom on the spheroid, there is very little shift in the position of zero tilt angle. However, there is a continual decrease in tilt angle at all stations, as shown in Figure 18. This data is plotted for the top centerline stations only since the curves for wing positions above the center at those stations gives the data for wing positions below the center for the bottom stations with tilt angle signs reversed. The curvature factor rises along the length of the spheroid as the wing is moved down. The intermediate wing positions cause only a general rise at all stations, while the extreme wing positions reveals the shielding effect of the wing when located at the top of the fuselage, and an opposite effect due to the increased fringing of the field to the fuselage when the wing is at the bottom.

Figure 19 shows the effect of varying the position of a wing having 35 degrees of sweep-back. Again the position of zero tilt angle

is nearly the same for all wing locations with a decrease in tilt angle that is evident only for stations forward of this position. Zero tilt angle occurs near the trailing edge of the wing in contrast to its location near the wing centerline for the straight wing. The overall shielding effect of the swept-back wing is apparent in the smaller changes in curvature factor at stations aft of the spheroid center as the wing position is changed. The largest variations in curvature factor occur at the forward stations and over the wing, resulting from localized shielding of the wing root.

The addition of the horizontal stabilizer (Figure 20) causes a shift of the tilt angle curve toward the tail and decreases the tilt angle in the vicinity of the stabilizer for both top and bottom stations. The curvature factor variation with position on the spheroid is very nearly the same as with the wing alone.

The vertical fin, which completes the simulated aircraft, produces the most marked effects, particularly on the curvature factor. Figure 21 shows that the tilt angle curve flattens out as the fin is approached along the top of the fuselage. A general decrease in tilt angle occurs at all the bottom stations aft of the wing. The curvature factor for the top stations decreases rapidly in the vicinity of the vertical fin, although for the high-wing configuration the general level and trends for the forward stations remain unchanged. The curvature factor for the low-wing position is reduced to the same level as for the mid-wing position. Along the bottom centerline the addition of the fin increases the curvature factor for the mid-wing position but decreases it for the high-wing position. At stations behind the wing the curvature factor for the low-wing

is nearly the same for all wing locations with a decrease in tilt angle that is evident only for stations forward of this position. Zero tilt angle occurs near the trailing edge of the wing in contrast to its location near the wing centerline for the straight wing. The overall shielding effect of the sweptback wing is apparent in the smaller changes in curvature factor at stations aft of the spheroid center as the wing position is changed. The largest variations in curvature factor occur at the forward stations and over the wing, resulting from localized shielding of the wing root.

The addition of the horizontal stabilizer (figure 20) causes a shift of the tilt angle curve toward the tail and decreases the tilt angle in the vicinity of the stabilizer for both top and bottom stations. The curvature factor variation with position on the spheroid is very nearly the same as with the wing alone.

The vertical fin, which completes the simulated aircraft, produces the most marked effects, particularly on the curvature factor. Figure 21 shows that the tilt angle curve flattens out as the fin is approached along the top of the fuselage. A general decrease in tilt angle occurs at all the bottom stations aft of the wing. The curvature factor for the top stations decreases rapidly in the vicinity of the vertical fin, although for the high-wing configuration the general level and trends for the forward stations remain unchanged. The curvature factor for the low-wing position is reduced to the same level as for the mid-wing position. Long the bottom symmetrical the addition of the fin increases the curvature factor the tilt-angle coefficient but decreases it for the high-wing position.

position is increased, making the shielding effect of the wing more pronounced.

Figures 22, 23, and 24 indicate the effect of wing sweepback for high, mid, and low-wing configurations. The shape of the tilt angle curve is similar for both wing styles at all three positions but a decided rearward shift is apparent for the swept-back wing. The general level of the curvature factor curves is the same at each wing position for both wing types. The swept-back wing causes a shift toward the tail of the maximum value of curvature factor at the high and mid-wing positions, and a shift rearward of the minimum value at the low-wing position.

Data obtained from a mock-up of a delta-wing aircraft is included in Figure 23. For top centerline stations the curvature factor is the same as for the straight wing configuration. The tilt angle is nearly the average of the values for straight and swept-back wings over the forward half of the fuselage. Along the bottom of the fuselage the curvature factor is again the same as for the straight wing. As the test station is moved rearward beneath the wing, a linear decrease in curvature factor occurs. When the trailing edge of the wing is reached the curvature factor rises abruptly.

Variations in vertical fin configuration were made at the low-wing position for both straight and swept-back wings. Figure 25 indicates a decrease in tilt angle at stations near the tail as the vertical fin area is increased. The addition of the three small fins causes a general increase in the curvature factor for both top and

position is increased, making the misleading effect of the wing more pronounced.

Figures 2), 23, and 24 indicate the effect of wing sweepback for high, mid, and low-wing configurations. The shape of the lift angle curve is similar for both wing styles at all these positions but a decided reversal shift is apparent for the swept-back wing. The general level of the curvature factor curves is the same at each wing position for both wing types. The swept-back wing curves a shift toward the tail of the maximum value of curvature factor at the high and mid-wing positions, and a shift rearward of the minimum value at the low-wing position.

Data obtained from a mock-up of a delta-wing aircraft is indicated in Figure 25. For top centerline stations the curvature factor is the same as for the straight wing configuration. The tail angle is nearly the average of the values for straight and swept-back wings over the forward half of the fuselage. Along the bottom of the fuselage the curvature factor is again the same as for the straight wing. As the boat section is moved rearward beneath the wing, a lower recovery in curvature factor occurs. When the trailing edge of the wing is reached the curvature factor rises abruptly.

Variations in vertical fin configuration were made of the low-wing position for both straight and sweep-back wings. Figure 26 [illegible] and crease in tail angle at about [illegible] The area [illegible] increased, making the misleading effect of the wing more pronounced.

bottom stations, while the large single fin affects only stations along the bottom of the fuselage particularly near the tail. The data for the swept-back wing presented in Figure 26 shows little effect on either quantity with a change in the vertical fin size.

2. Predictions and Measurements on Aircraft Models

The results so far have been general, in that they deal with a simulated aircraft whose components were determined from the average of a number of actual aircraft. Since the intent of this study is to increase the accuracy in predicting the characteristics of a particular aircraft, these general results were used to predict the variations in curvature factor and tilt angle for five different representative aircraft.

The method of using the general curves for prediction is best illustrated by describing the step-by-step procedure for predicting the characteristics of the P2V aircraft. The P2V is a twin-engine aircraft having a large single vertical tail. The wing location is between the mid-wing and high mid-wing configurations simulated with the prolate spheroid. Interpolation of the curves for mid-wing and high-wing configurations in Figure 14 should take into account all the airframe variations except for the nacelles. The amount of interpolation for the wing position is indicated by the curves of Figure 11 for the wing alone on the spheroid. Figures 9 and 10 indicate an effect due to the nacelles on the fuselage stations nearest the nacelles. Because of the central location of the P2V wing, the effect on the curvature factor will in all probability be small and apparent only at the top stations which

are adjacent to the nacelles.

Comparisons of the actual model measurements with the predicted characteristics are shown in Figures 20 through 24 for the five aircraft. The curves indicate an ability to predict the shape of the curvature factor and tilt angle curves. The prediction of the cross-over point for the tilt angle and the general level of the curvature factor is influenced largely by departures in detail of configuration from the idealized model used for simulation.

One effect of these details appears in Figure 20 with the low curvature factor on both the top and the bottom of the fuselage. This is attributable to the flattened cross-section of the P2V fuselage. The location of an antenna on a surface for which the radius of curvature is small relative to the antenna size results in a radical departure of the curvature factor from the predicted value. This effect is illustrated in the curves for the DC-6, F-84, and F-86 models by the sharp rise in curvature factor at stations near the tail due to dorsal extension of the vertical fins.

The tilt angle curves for all the aircraft fall forward of the predicted curves. This is reasonable since the aircraft tend more toward a tear-drop fuselage shape in longitudinal cross-section than to the symmetry of the spheroid.

are adjacent to the nacelles.

Comparisons of the actual model measurements with the predicted characteristics are shown in Figures 20 through 24 for the five aircraft. The curves indicate an ability to predict the shape of the curvature factor and tilt angle curves. The prediction of the cross-over point for the tilt angle and the general level of the curvature factor is influenced largely by departures in detail of configuration from the idealized model used for simulation.

One effect of these details appears in Figure 20 with the low curvature factor on both the top and the bottom of the fuselage. This is attributable to the flattened cross-section of the XC-142 fuselage. The location of an antenna on a surface for which the radius of curvature is small relative to the antenna size results in a radical departure of the curvature factor from the predicted value. This effect is illustrated in the curves for the DC-6, F-8A, and T-8B models by the sharp rise in curvature factor at stations near the tail due to dorsal extension of the vertical fins.

The tilt angle curves for all the aircraft fall forward of the predicted curves. This is reasonable since the aircraft tend more toward a tear-drop fuselage shape in longitudinal cross-section than to the symmetry of the spheroid.

CHAPTER VI

CONCLUSIONS

This study provides much information of a general nature concerning low-frequency aircraft antenna characteristics. Explicit trends due to the configuration are clearly indicated. The longitudinal position of the wing largely determines the location of zero tilt angle, though this is influenced slightly by the size and shape of the tail assembly. The vertical position of the wing is the controlling factor in the general level of the curvature factor for both top and bottom stations. The curvature factor will be higher on the top or the bottom of the fuselage depending on which is farther from the plane of the wing. Sweepback in the wing plan-form causes the localized effects in the region of the wing root to spread over a greater length of the fuselage. The vertical fin size is the predominant factor in the localized effects at stations near the tail. As the size is increased the curvature factor decreased more rapidly on the top of the fuselage in the vicinity of the fin. The tilt angle decreases less rapidly near the tail with an increase in the vertical fin size. The nacelles provide only localized effects on the stations nearest them.

The comparison of the actual model measurements with the predictions based on the general curves indicates the need for more information concerning the smaller details of the aircraft configuration. The predictions are not sufficiently accurate for use as design information unless modified to include these effects. The modifications to the

CHAPTER VI

CONCLUSIONS

This study provides much information of a general nature concerning low-frequency aircraft antenna characteristics. Explicit trends due to the configuration are clearly indicated. The longitudinal position of the wing largely determines the location of zero tilt angle, though this is influenced slightly by the size and shape of the tail assembly. The vertical position of the wing is the controlling factor in the general level of the curvature factor for both top and bottom stations. The curvature factor will be higher on the top or the bottom of the fuselage depending on which is farther from the plane of the wing. Sweepback in the wing plan-form causes the localized effects in the region of the wing root to spread over a greater length of the fuselage. The vertical fin size is the predominant factor in the localized effects at stations near the tail. As the size is increased the curvature factor decreased more rapidly on the top of the fuselage in the vicinity of the fin. The tilt angle increases less rapidly near the tail with an increase in the vertical fin size. The nacelles provide only localized effects on the stations nearest them.

The comparison of the actual model measurements with the predictions based on the general curves indicates the need for more information concerning the smaller details of the aircraft configuration. The predictions do not sufficiently accurate for use as design information unless modified to include the nacelle effects. The modifications to the

basic information can be obtained by continual comparison of the curves for specific aircraft with the general curves. In this manner the effects of the smaller details in configuration may be identified and used to provide more accurate predictions. Further employment of the electrostatic measurement technique in the study of low-frequency aircraft antenna characteristics should include a program of correlation with this basic study to enhance its value as a design tool.

BIBLIOGRAPHY

1. Bolljahn, J. T. Antennas for Airborne ADF Systems. Interim Engineering Report on Task II, Stanford Research Institute Project No. 206, Air Force Contract No. AF 33(038)7850. February 1952.

2. Bolljahn, J. T. Small Dipole-type Antennas. Technical Report No. 14, Stanford Research Institute Project No. 188, Air Force Contract No. AF 19(122)78. September 1950.

3. Bolljahn, J. T. The Measurement of Low-frequency Aircraft Antenna Properties using Electrostatic Techniques. Technical Report No. 19, Stanford Research Institute Project No. 188, Air Force Contract No. AF 19(122)78. September 1951.

4. Hoblitzell, C. M. Effect of Airframe Configuration on Low-frequency Antenna Characteristics. Technical Report No. 38, Stanford Research Institute Project No. 591, Air Force Contract No. AF 19(604)266. April 1953.

5. Reese, R. F. Radio Compass Flush-mounted Sense Antenna Installation in the Boeing B-47 Aircraft. Final Report, Stanford Research Institute Project No. 762, Boeing Airplane Company Purchase Order No. 525701-952. February 1953.

6. Smythe, W. R. Static and Dynamic Electricity. McGraw-Hill New York. 1939.

1. Bolljahn, J. T. [illegible] for Airborne ADF Systems. [illegible]
[illegible] Report on Task II, Contract No. [illegible]
Project No. 2[illegible], Air Force Contract [illegible].
February 1[illegible].

2. Bolljahn, J. T. Small Dipole-type Antennas. Technical Report
No. 2, Stanford Research Institute Project No. [illegible], Air
Force Contract No. AF 19(122)76. September 1950.

3. Bolljahn, J. T. The Measurement of Low-Frequency Airborne
Antenna Impedance using Electrostatic Tuning Vanes. Technical
Report No. 3, Stanford Research Institute Project No. [illegible],
Air Force Contract No. AF 19(122)76. September 1951.

4. Hollister, J. [illegible] of Airframe Configuration on Low-
Frequency Antenna Characteristics. Technical Report No. 38,
Stanford Research Institute Project No. 537, Air Force
Contract No. AF 19(604)455. April 1953.

5. Jones, R. V. Radio Corpora Multi-mounted Aerial Installation
in the Boeing B-47 Aircraft. Final Report, Stanford Research
Institute Project No. 701, Boeing Airplane Company Purchase
Order No. 52970(0-)52. February 1952.

6. Smythe, W. R. Static and Dynamic Electricity. McGraw-Hill
New York. 1939.

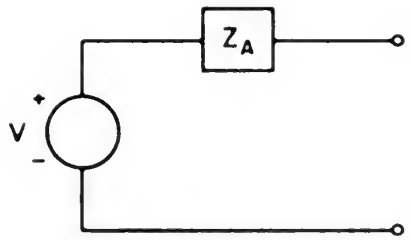

FIG. 1

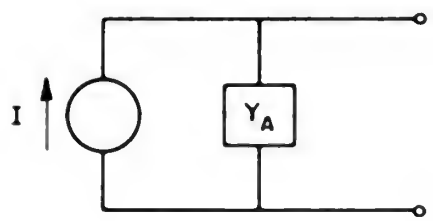

FIG. 2

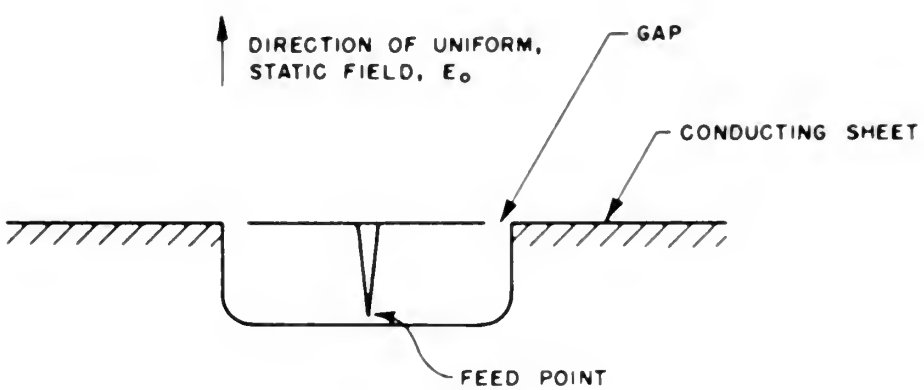

FIG. 3

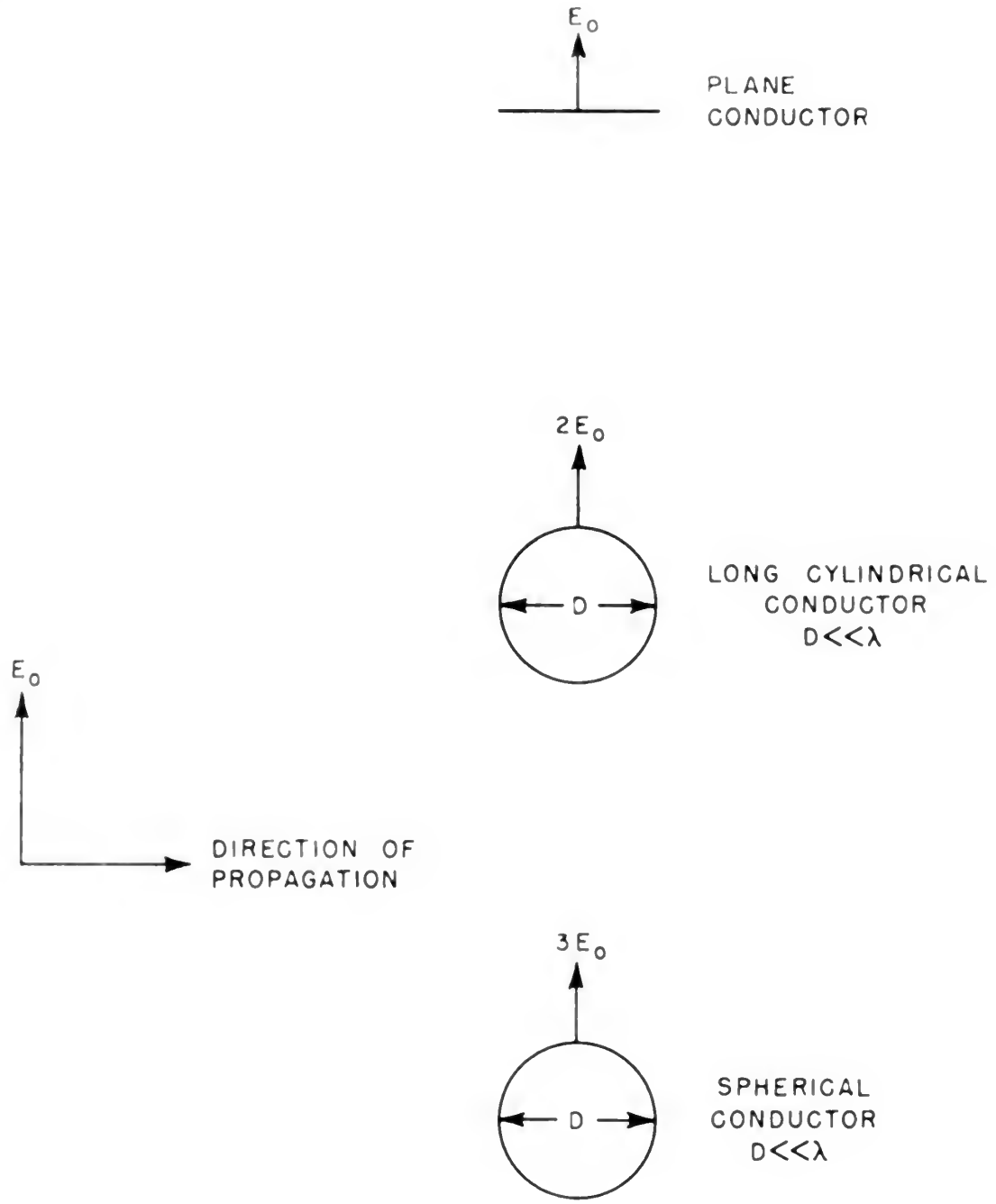
E_0
PLANE
CONDUCTOR
$2E_0$
D
LONG CYLINDRICAL
CONDUCTOR
D<<λ
E_0
DIRECTION OF
PROPAGATION
$3E_0$
D
SPHERICAL
CONDUCTOR
D<<λ

FIG. 4

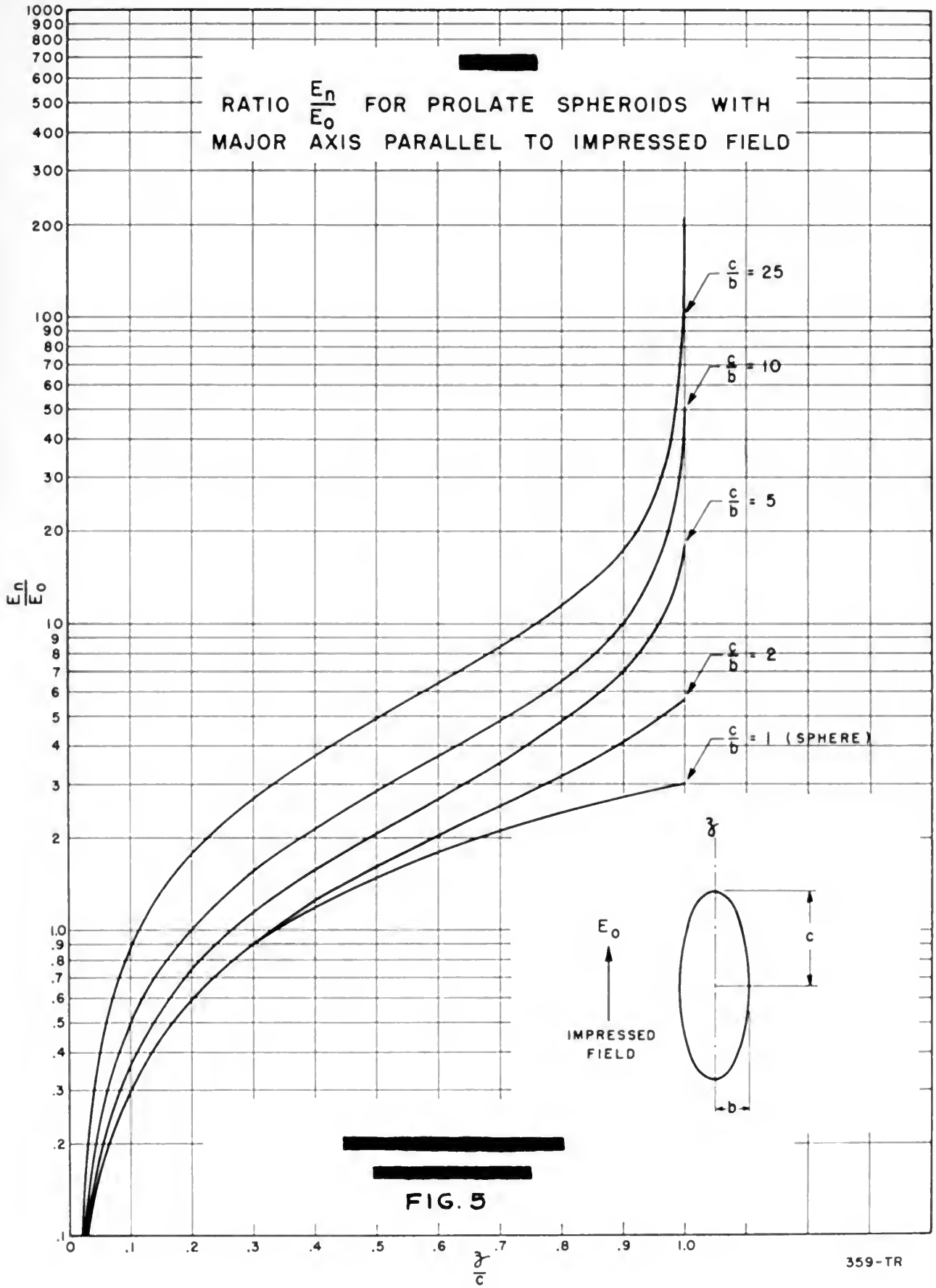
RATIO $\frac{E_n}{E_o}$ FOR PROLATE SPHEROIDS WITH MAJOR AXIS PARALLEL TO IMPRESSED FIELD
$\frac{c}{b}$ = 25
$\frac{c}{b}$ = 10
$\frac{c}{b}$ = 5
$\frac{c}{b}$ = 2
$\frac{c}{b}$ = 1 (SPHERE)
$\frac{E_n}{E_o}$
$\frac{z}{c}$
E_o
IMPRESSED FIELD
z
c
b
359-TR

FIG. 5

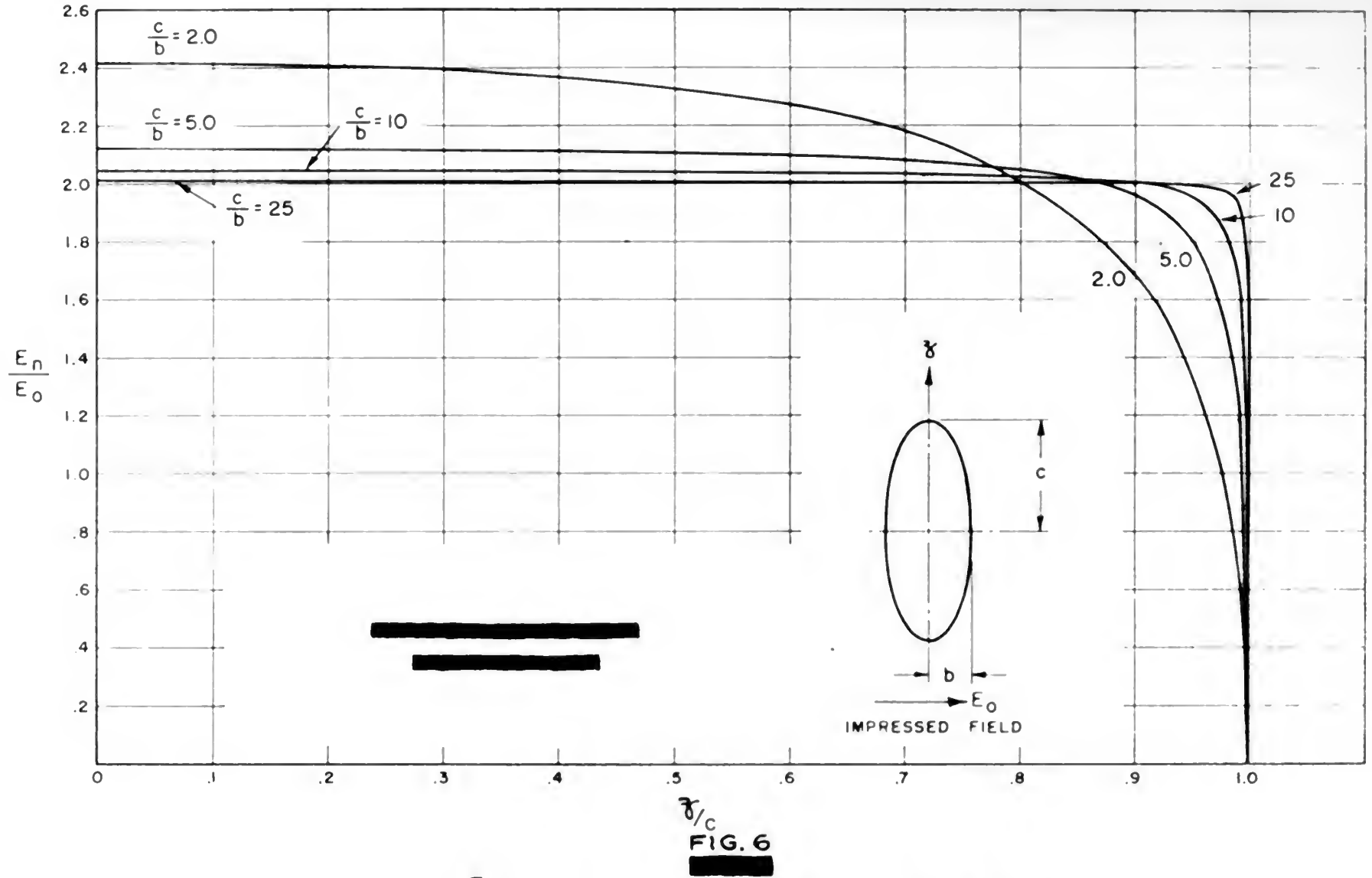

FIG. 6

RATIO $\frac{E_n}{E_o}$ FOR PROLATE SPHEROIDS WITH MAJOR AXIS PERPENDICULAR TO IMPRESSED FIELD

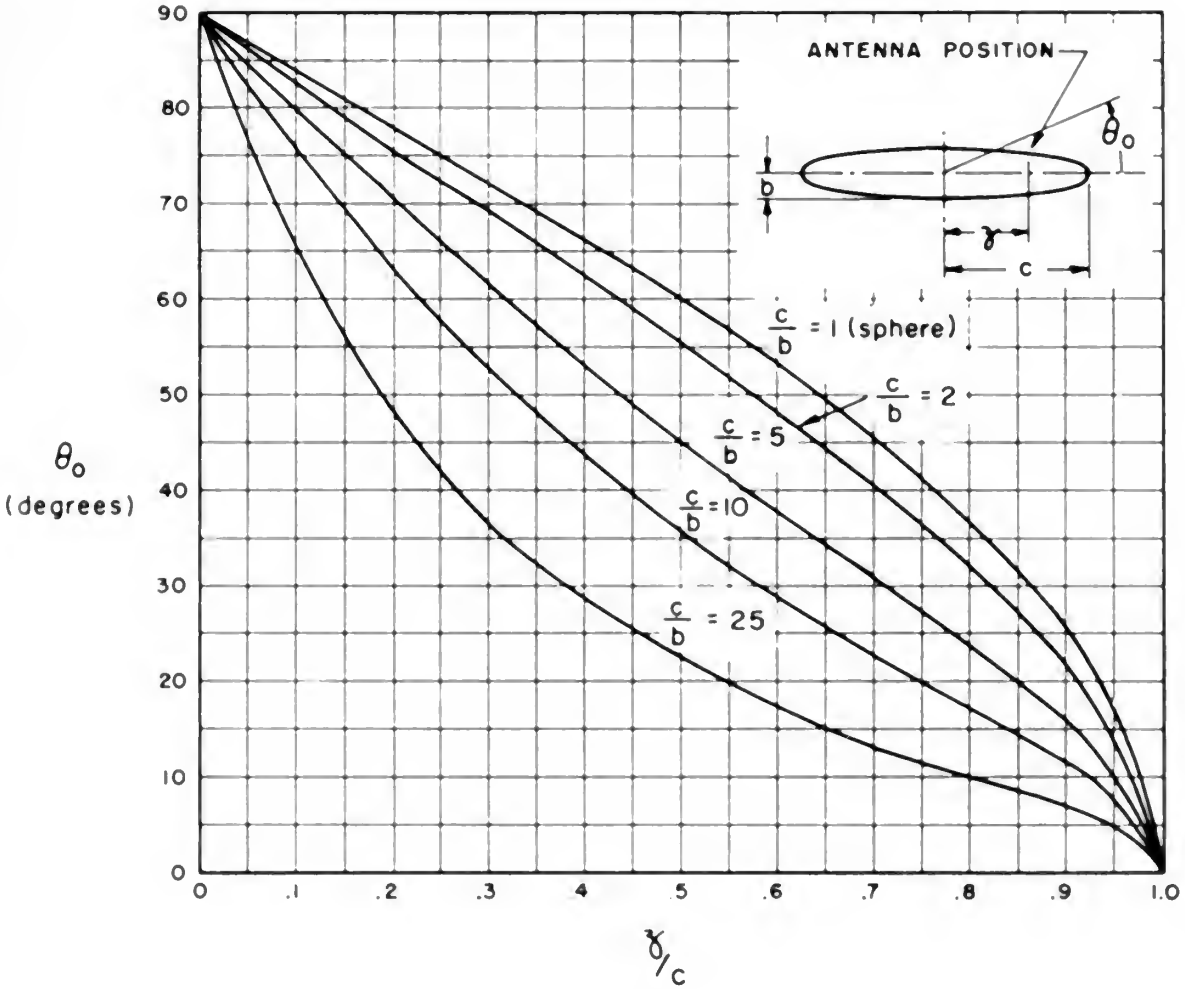

FIG. 7

ANGLE OF RADIATION NULL
FROM FLUSH ANTENNA ON SMALL
PROLATE SPHEROID

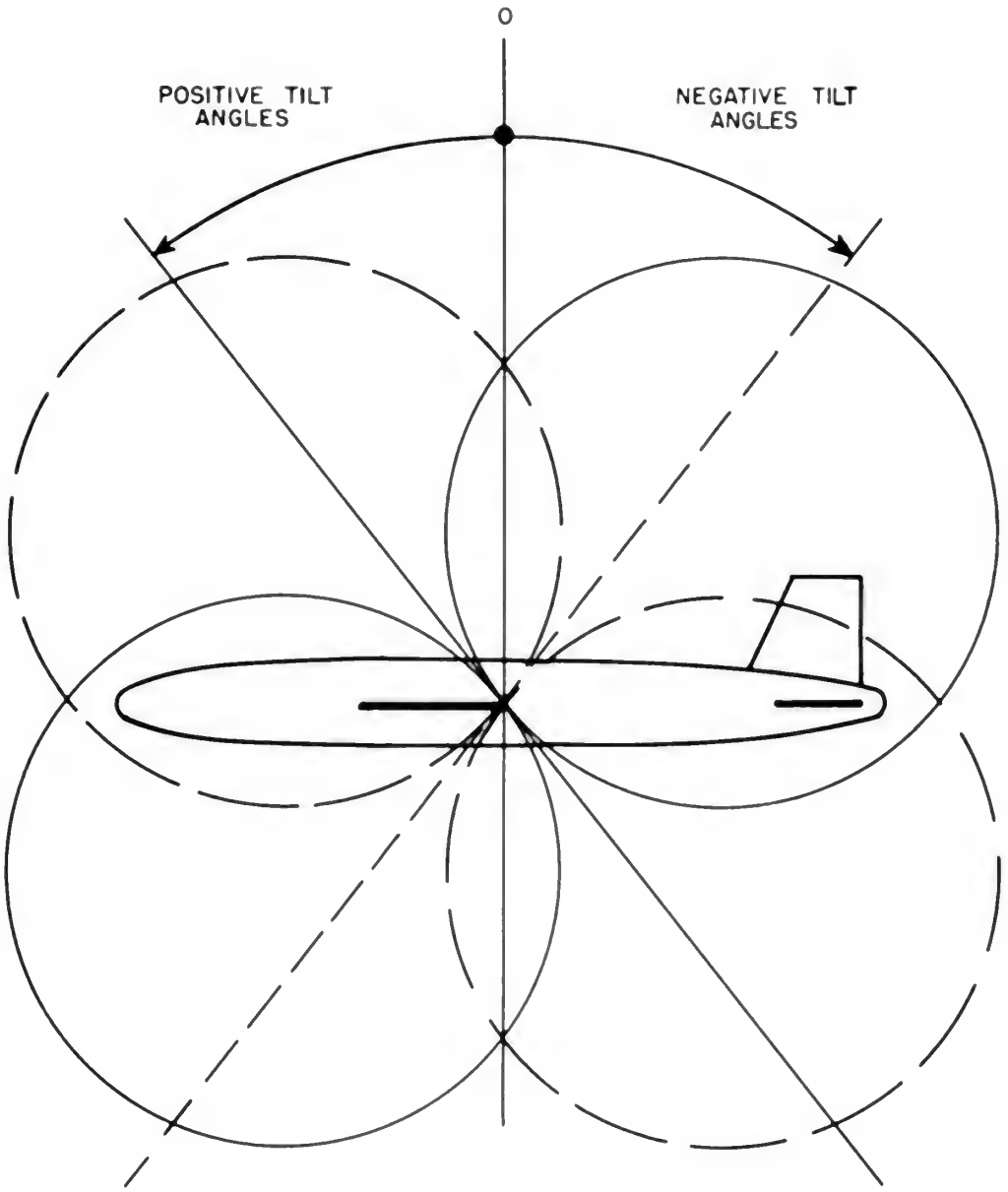

FIG. 8

TYPICAL AIRCRAFT RADIATION PATTERN

IA-591-TR38-178

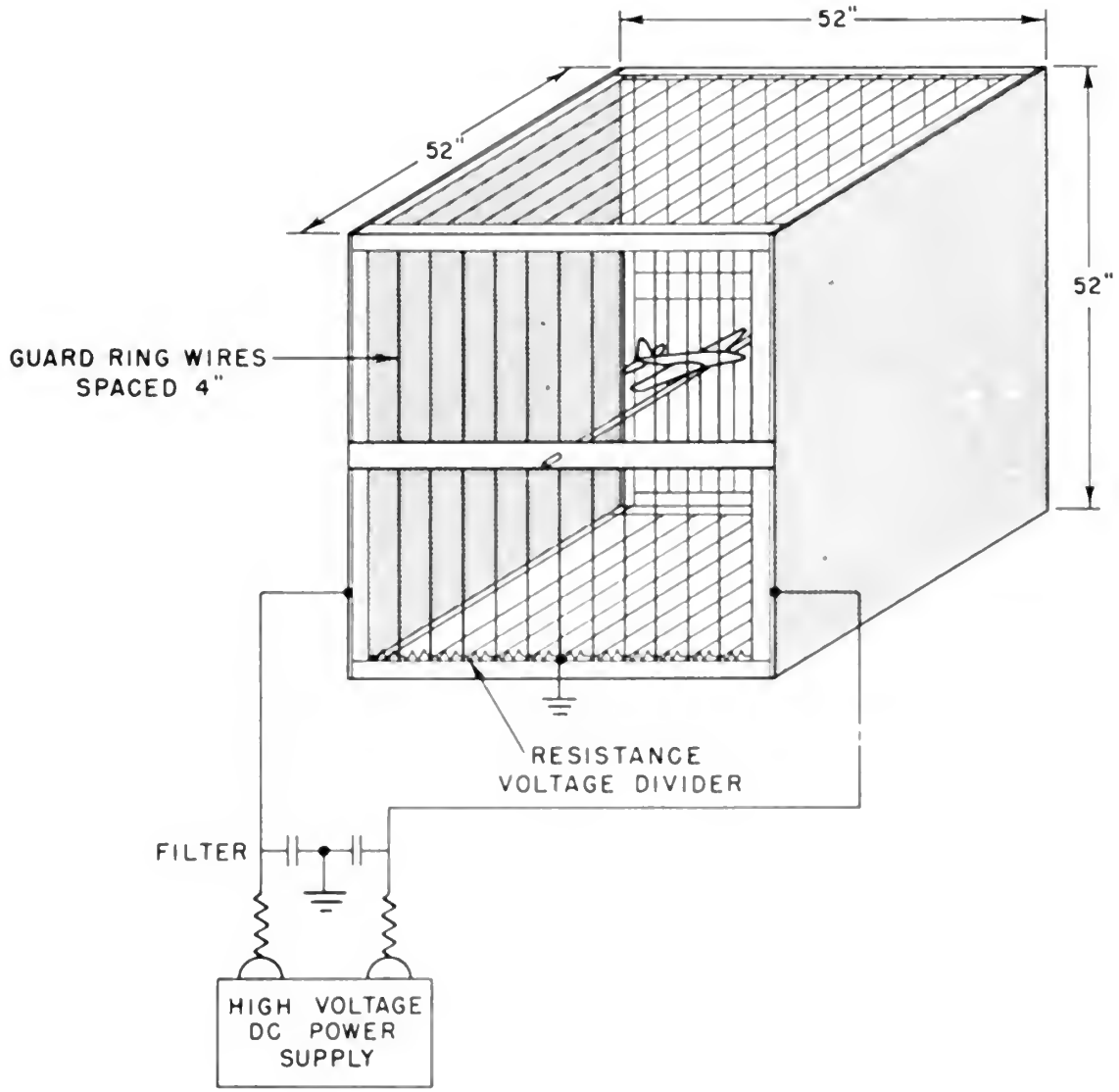

FIG. 9

ELECTROSTATIC CAGE

IA-188-18

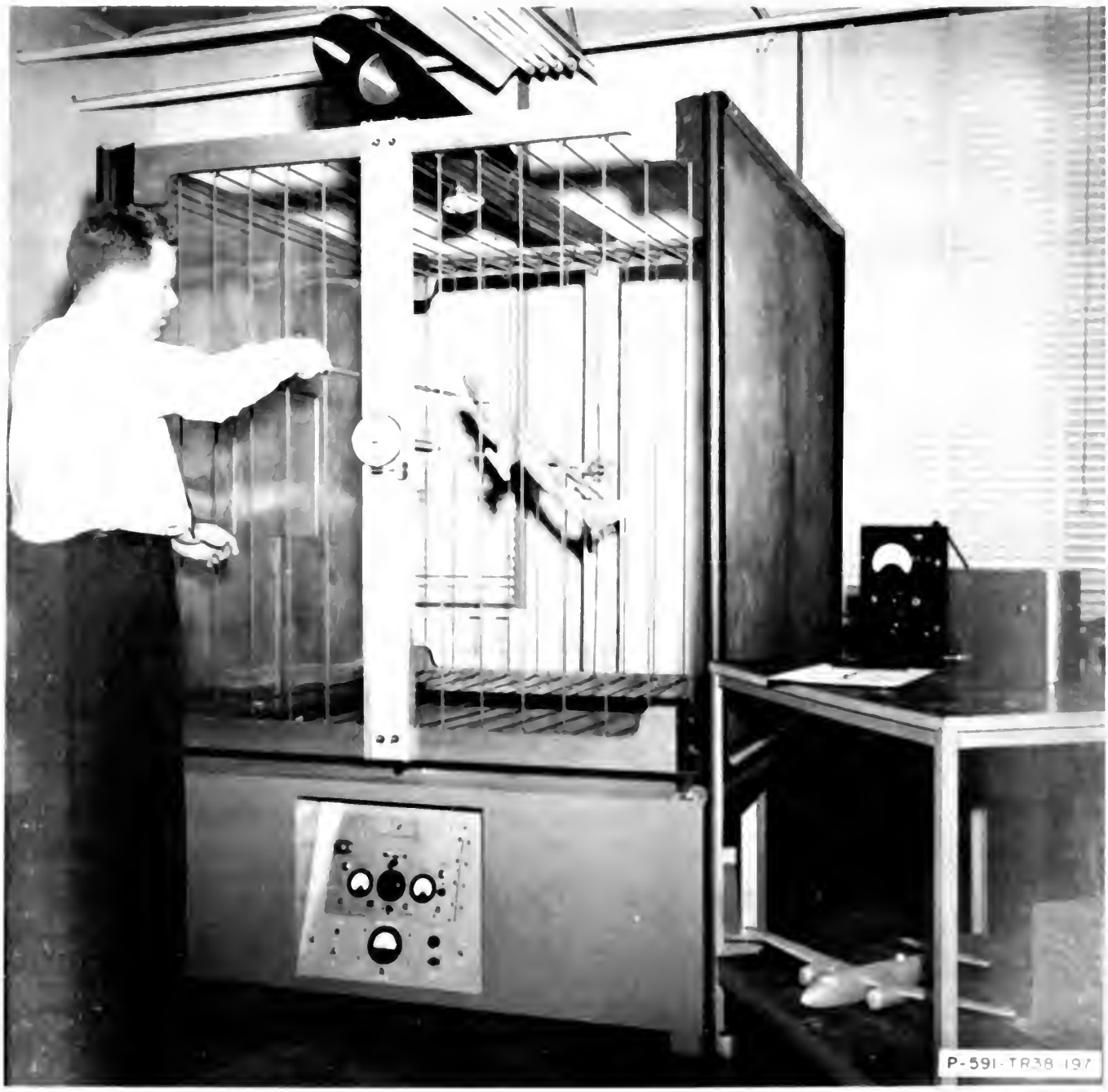

FIG. 10

ELECTROSTATIC MEASUREMENT FACILITIES

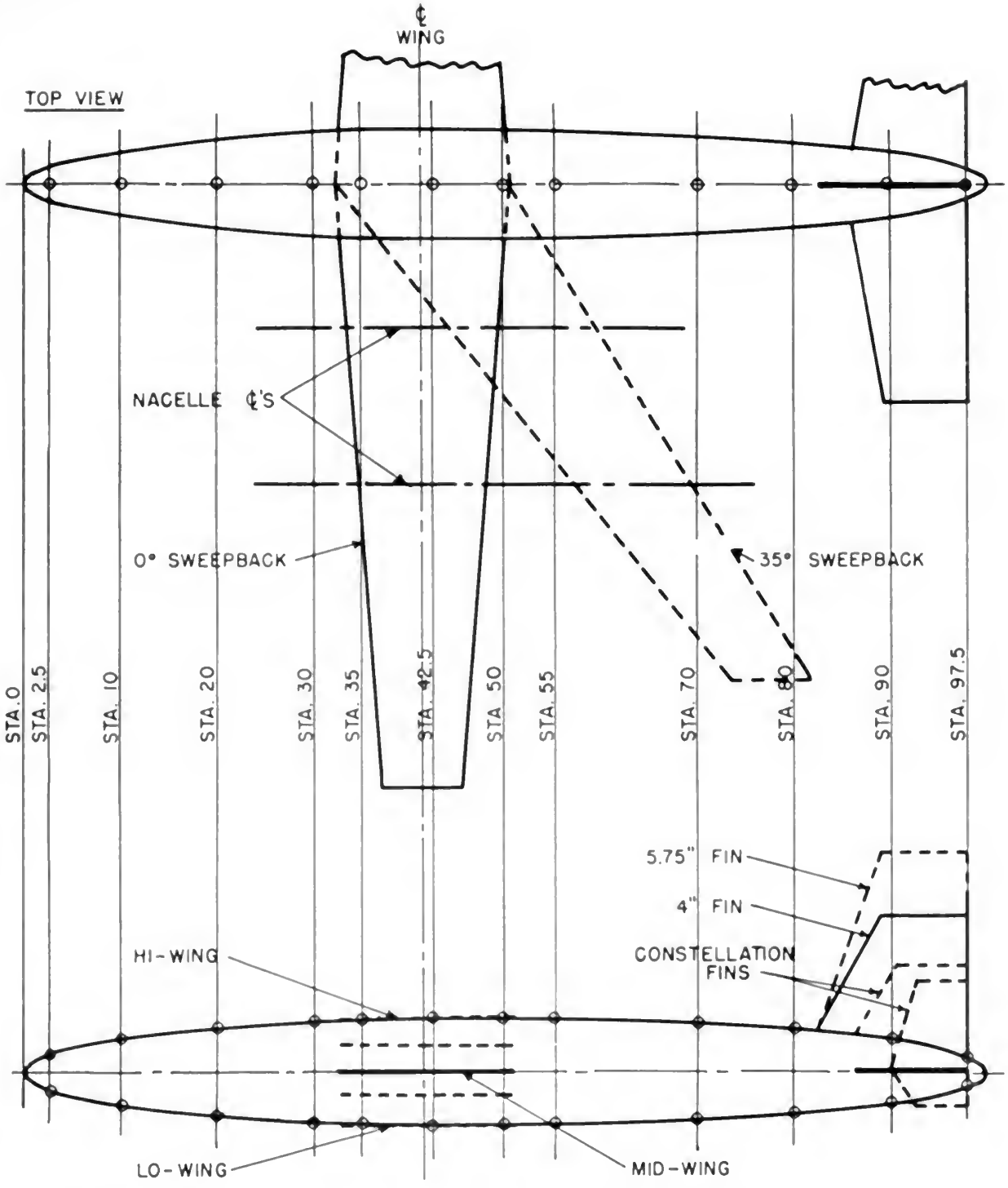

NOTE: O INDICATES LOCATION OF TEST POSITION.
STATION NUMBERS INDICATE % OF FUSELAGE LENGTH.
SCALE: $\frac{1}{4}$" = 1"

FIG. 11

PROLATE SPHEROID MODEL SHOWING TEST STATIONS AND VARIOUS CONFIGURATIONS

IA-591-TR38-179

FIG. 12

PROLATE SPHEROID MOCK-UP OF SWEPT-BACK HIGH WING AIRCRAFT

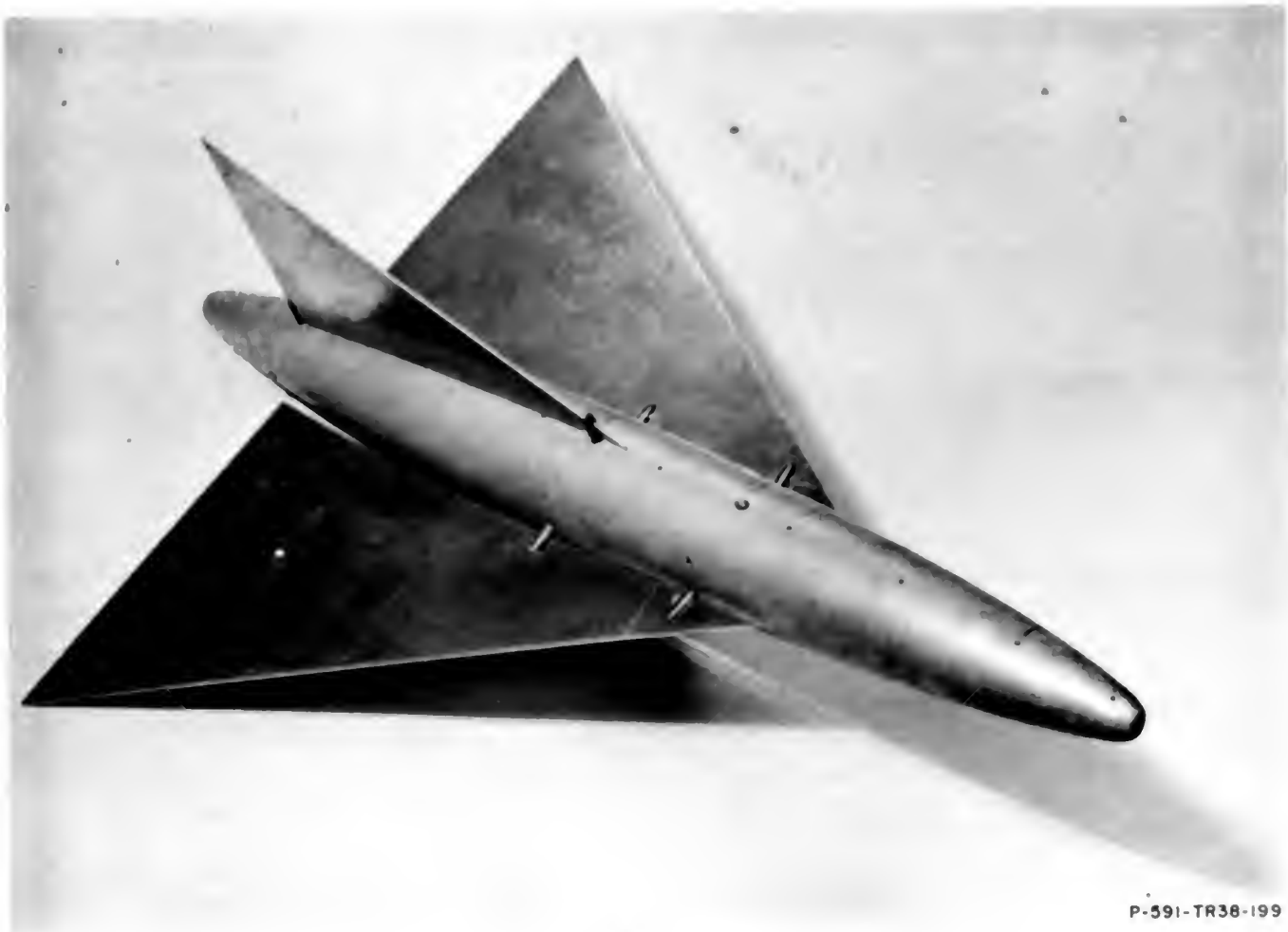

FIG 13

PROLATE SPHEROID MOCK-UP OF DELTA WING AIRCRAFT

FIG. 14

PROLATE SPHEROID MOCK-UP OF LOW WING
MULTI-ENGINE AIRCRAFT

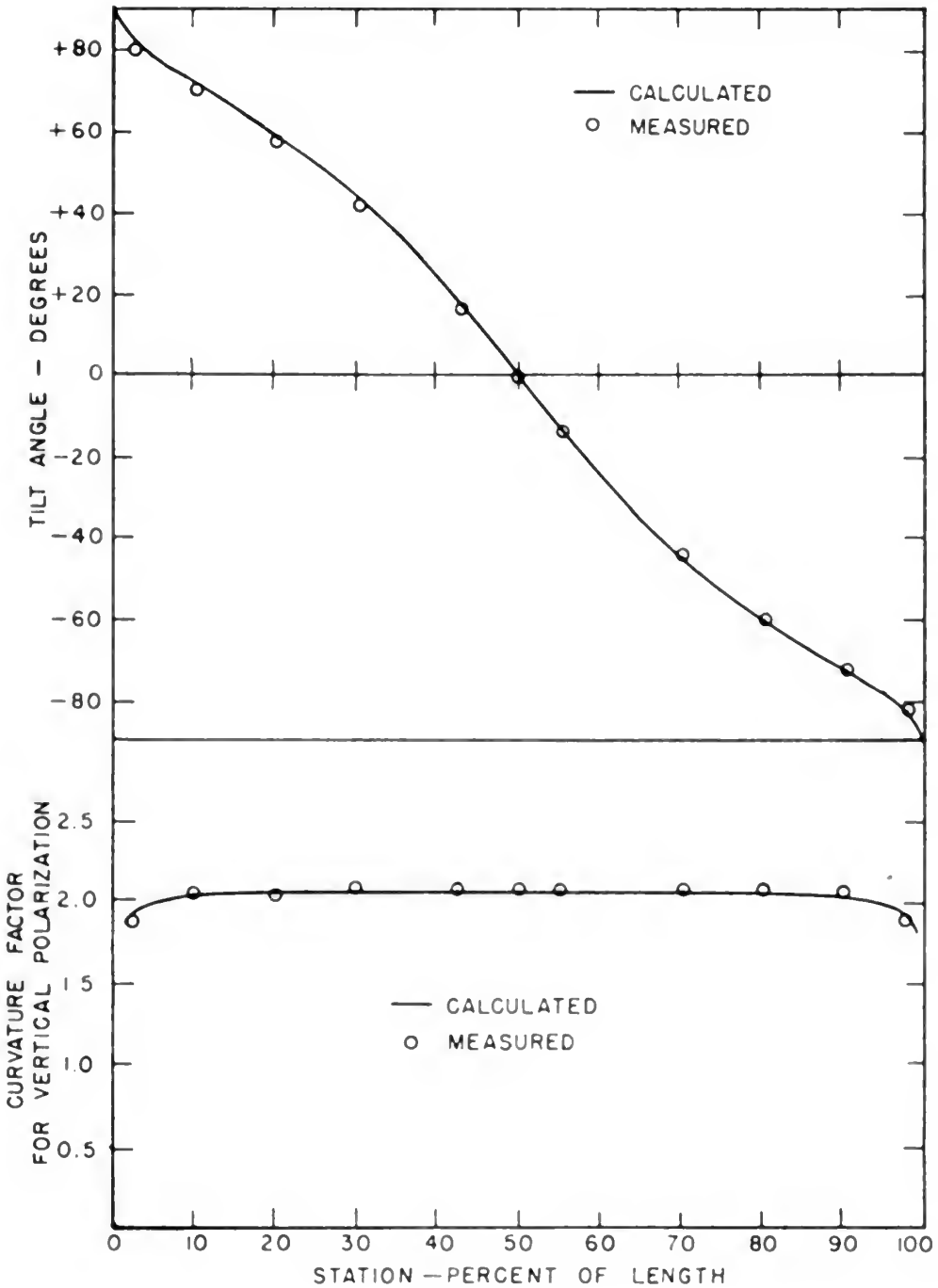

FIG. 15

CURVATURE FACTOR AND TILT ANGLE FOR A SMALL ANTENNA ON A PROLATE SPHEROID HAVING A MAJOR-TO-MINOR AXIS RATIO OF 9

IA-591-TR38-180

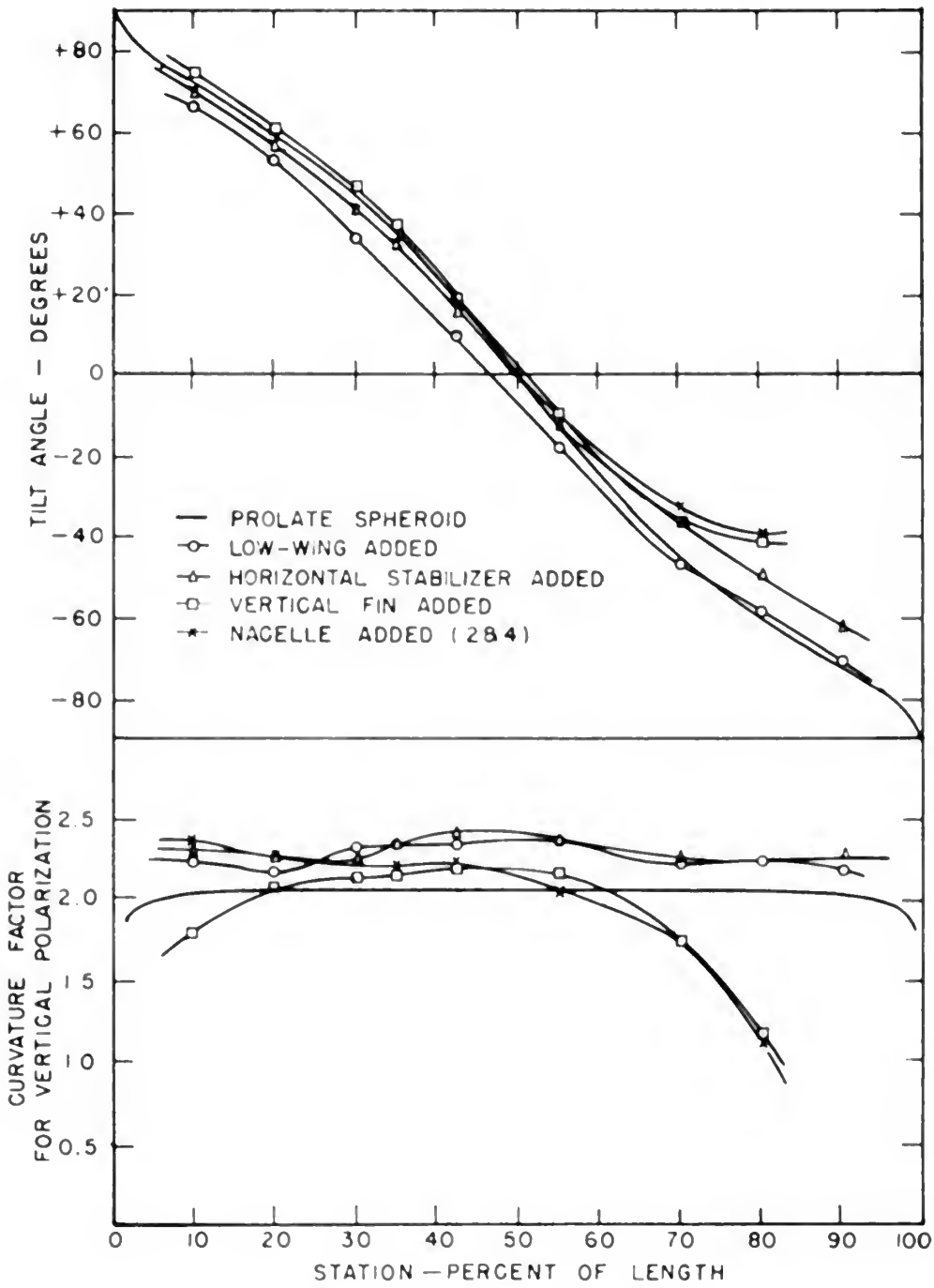

FIG. 16

EFFECT OF MAJOR AIRFRAME COMPONENTS
TOP CENTERLINE STATIONS

IA-591-TR38-181

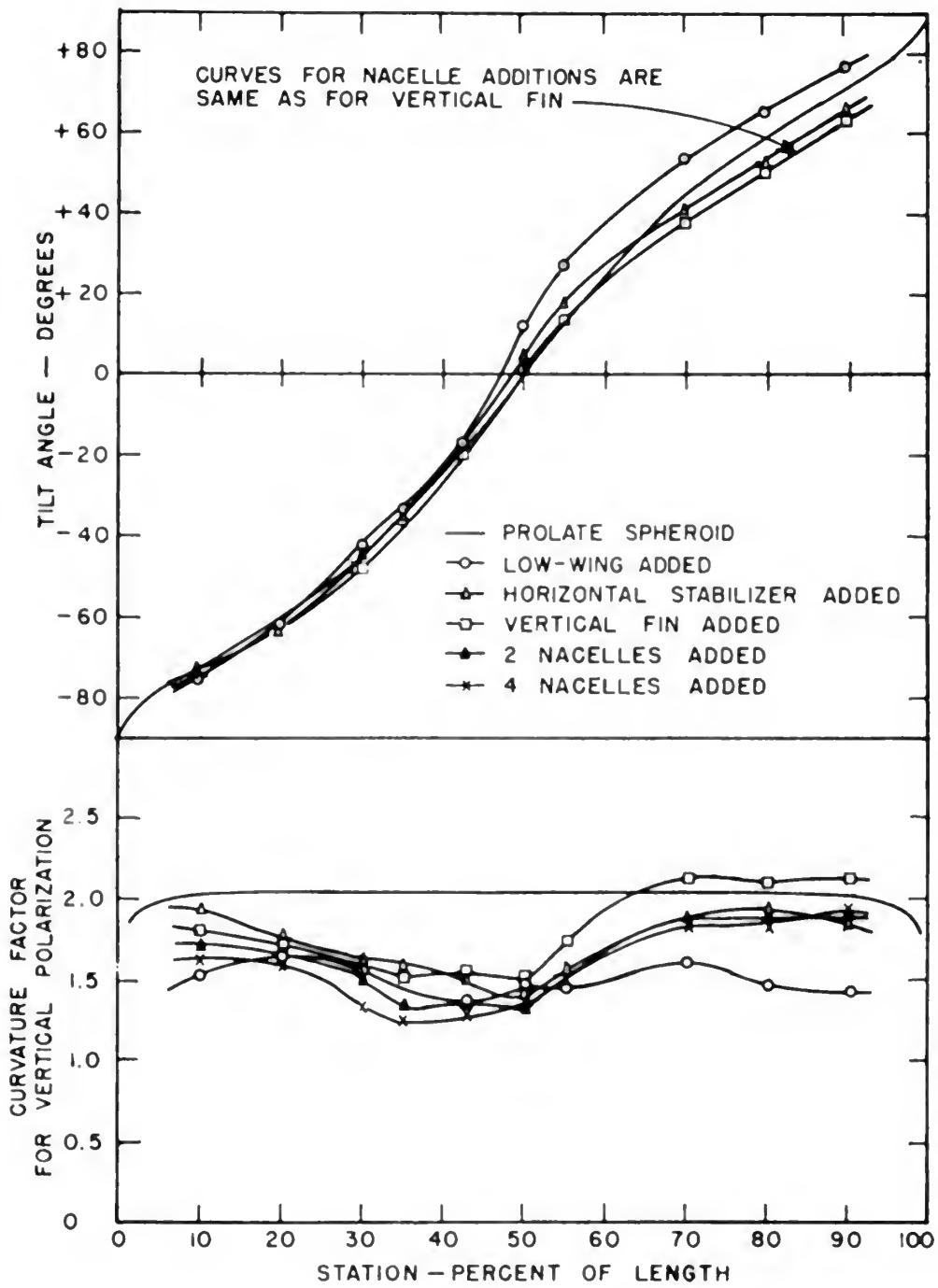

FIG. 17

EFFECT OF MAJOR AIRFRAME COMPONENTS
BOTTOM CENTERLINE STATIONS

IA-591-TR38-182

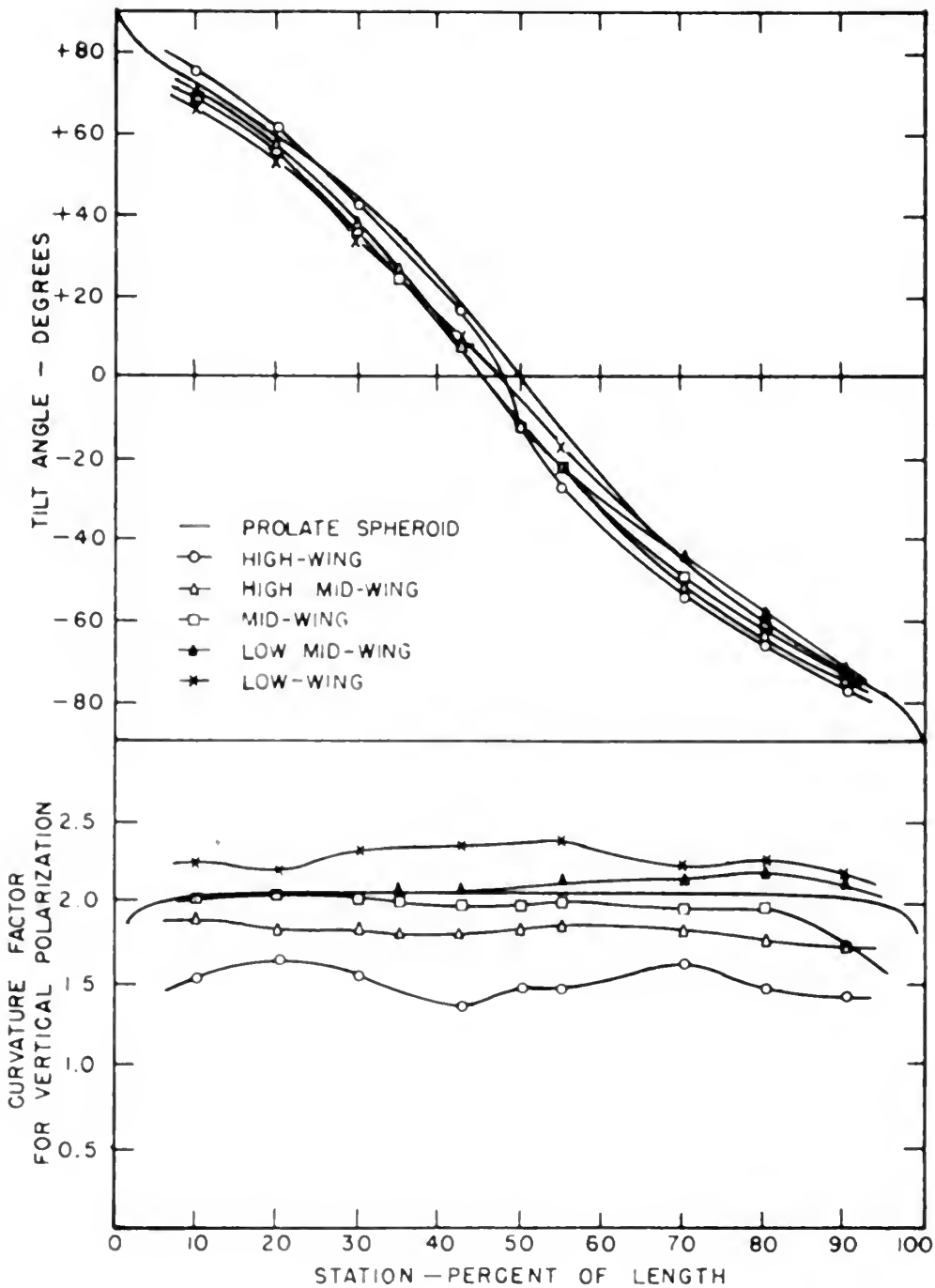

FIG. 18

EFFECT OF WING POSITION ON SPHEROID ONLY
(0° SWEEPBACK)

IA-591-TR38-183

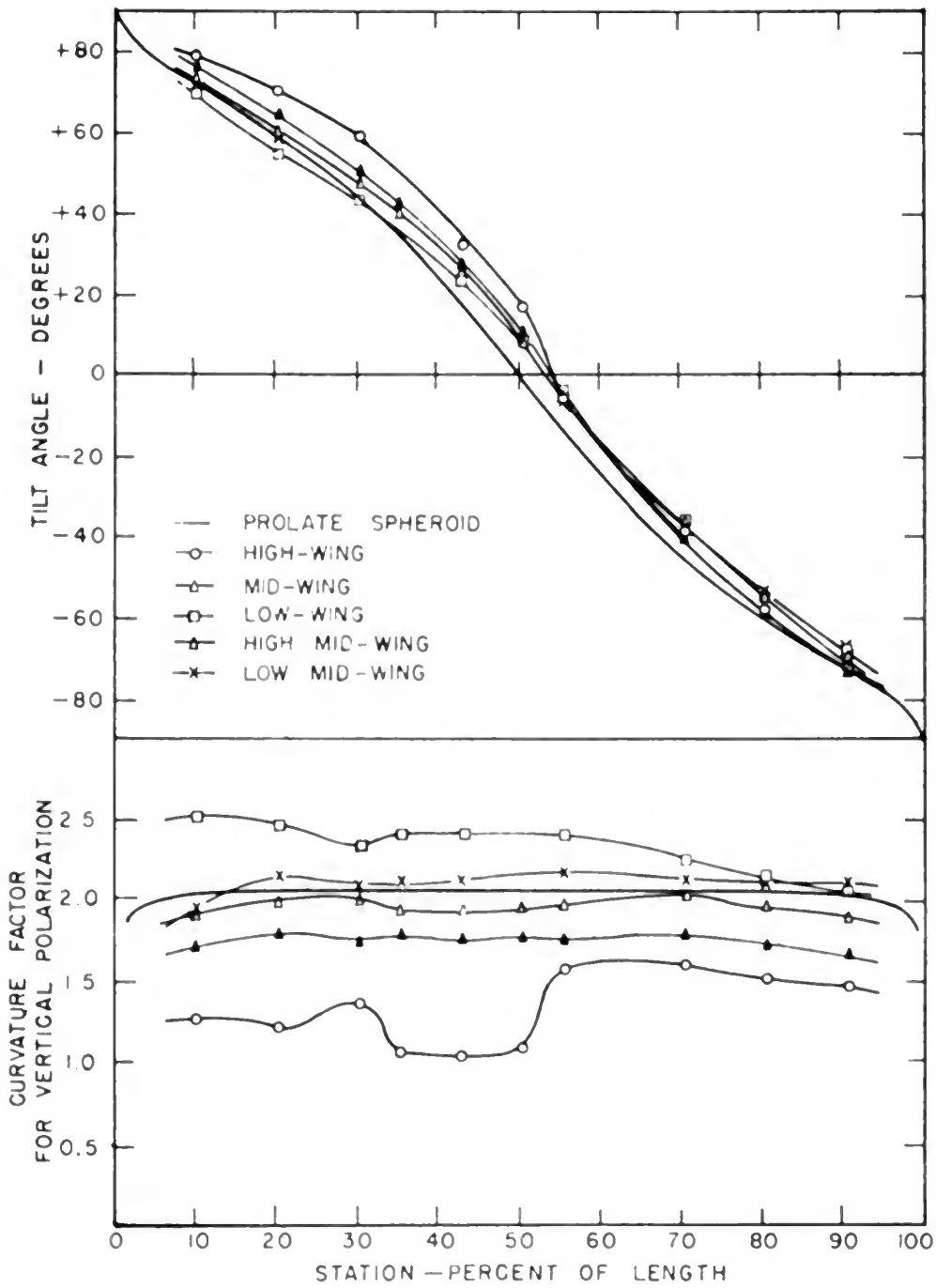

FIG. 19

EFFECT OF WING POSITION ON SPHEROID ONLY
(35° SWEEPBACK)

IA-591-TR38-184

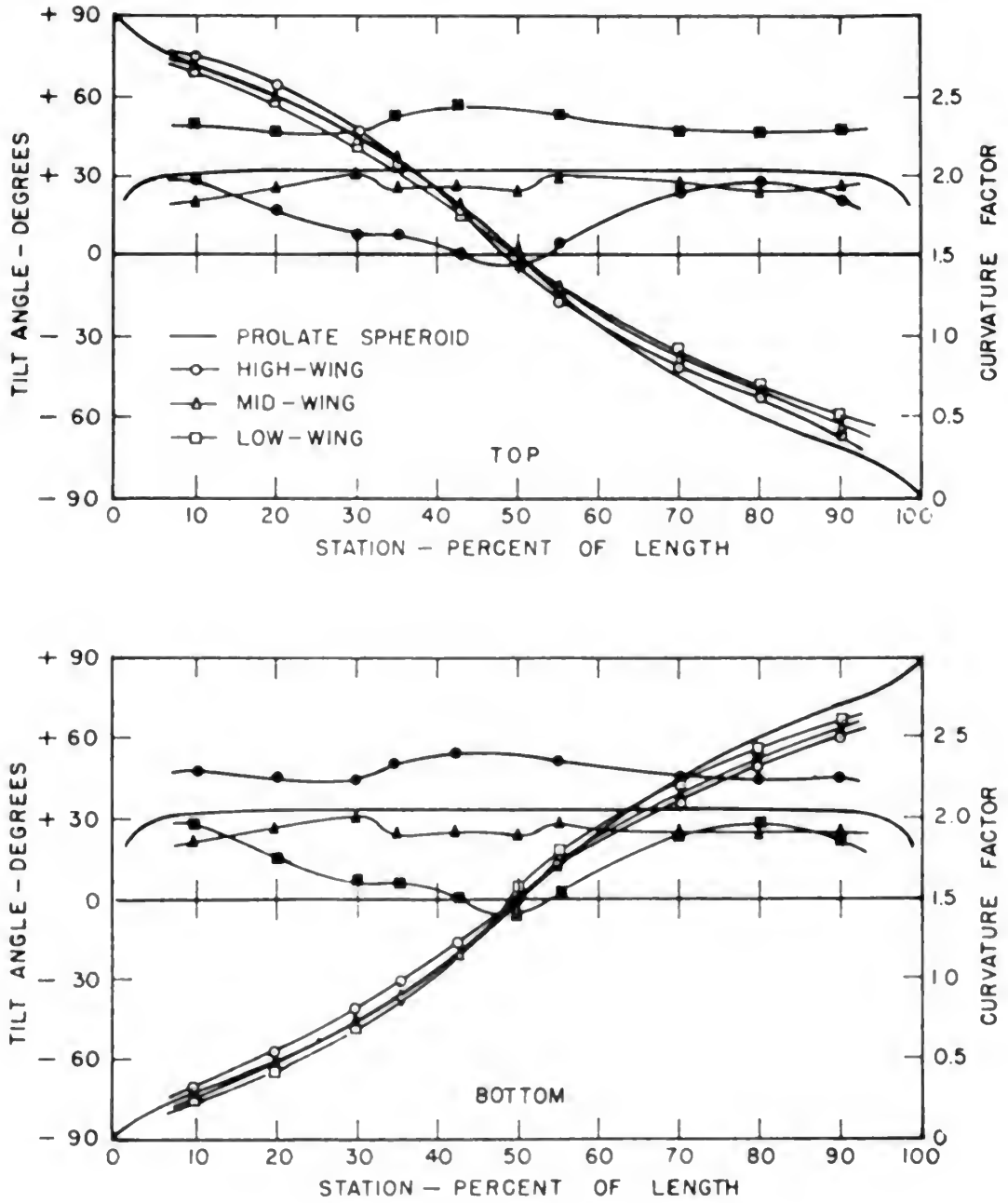

FIG. 20

EFFECT OF WING POSITION ON SPHEROID
WITH HORIZONTAL STABILIZER
(0° SWEEPBACK)

IA-591-TR38-185

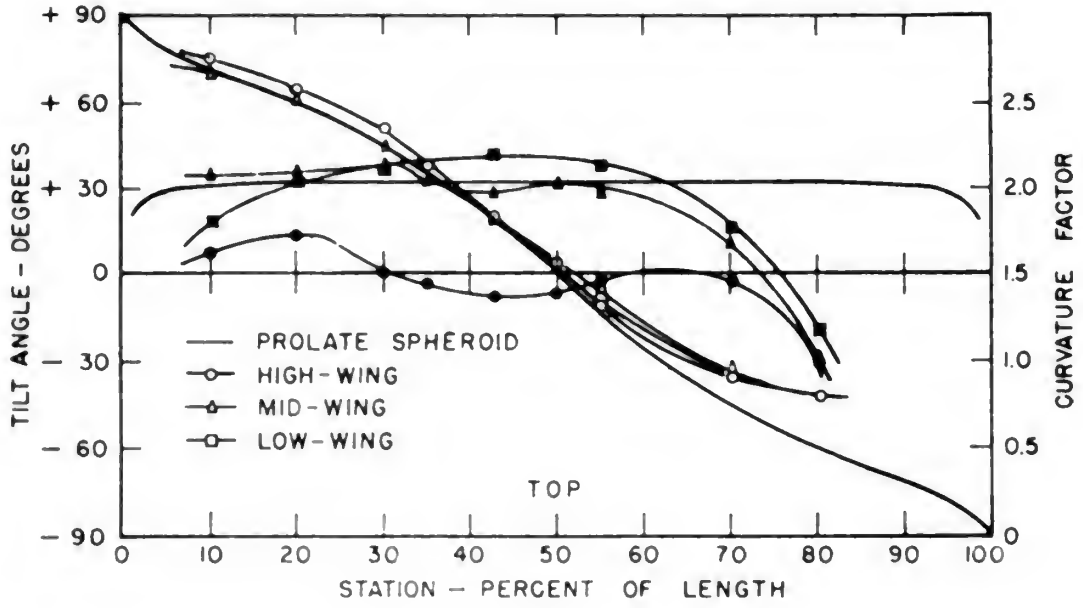

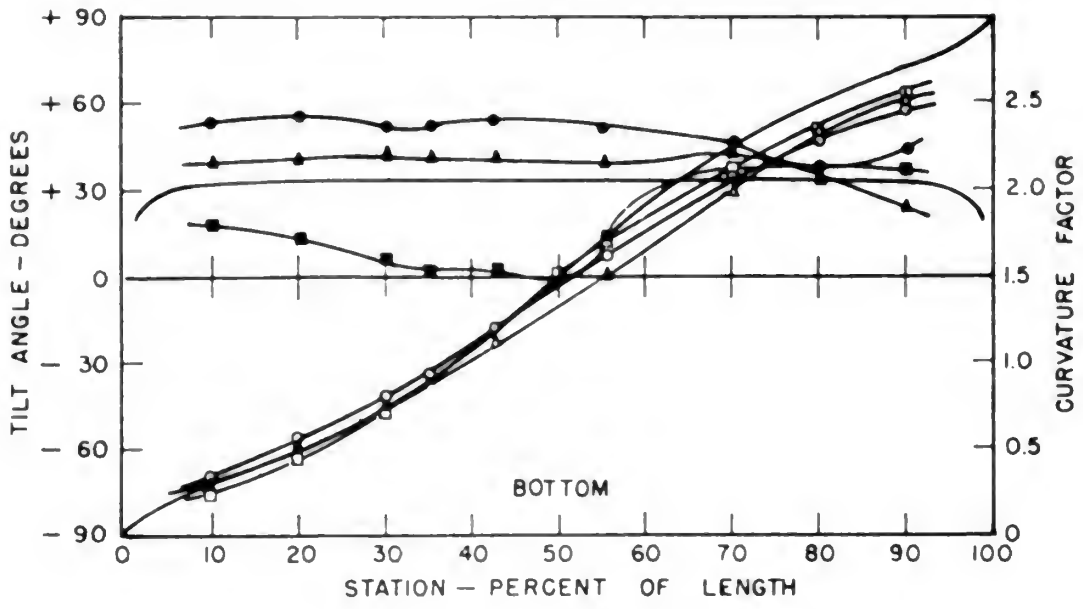

FIG. 21

EFFECT OF WING POSITION ON SPHEROID
WITH HORIZONTAL STABILIZER AND LARGE VERTICAL FIN
(0° SWEEPBACK)

IA-591-TR38-186

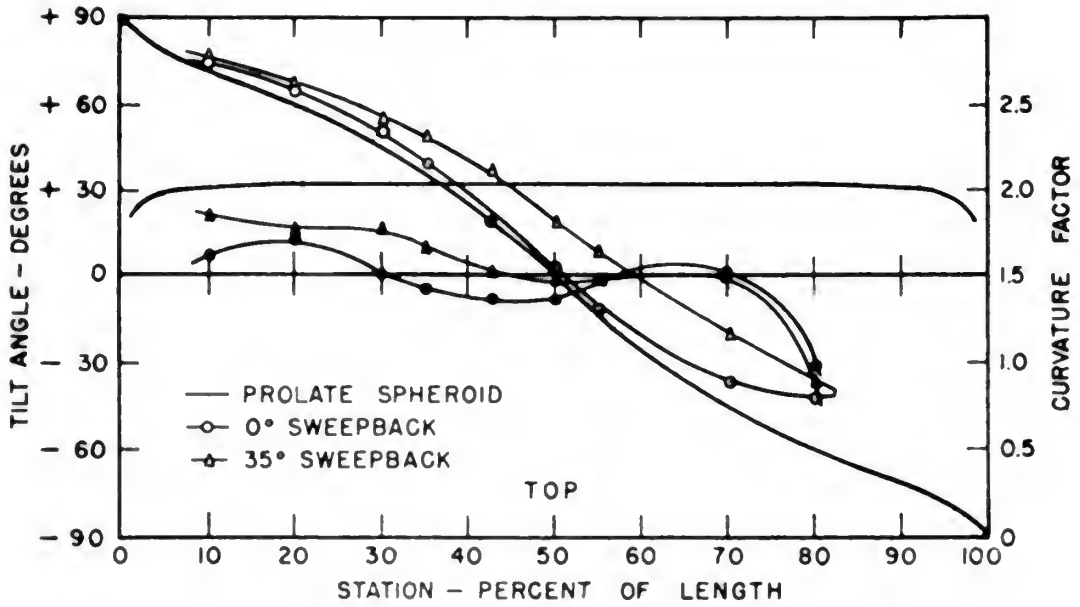

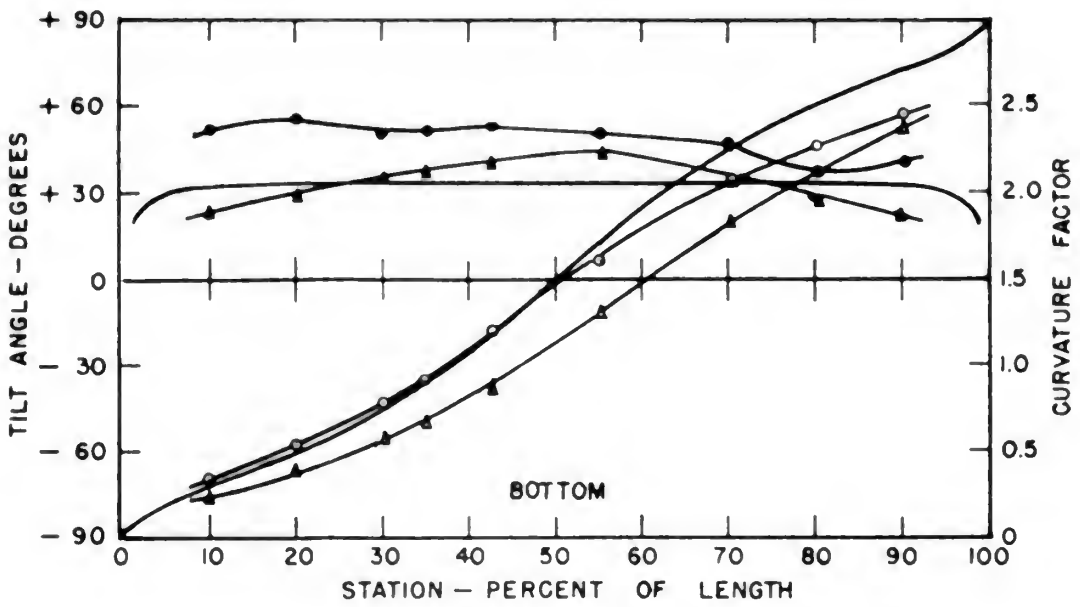

FIG. 22

EFFECT OF SWEEPBACK AT HIGH WING POSITION

IA-591-TR38-187

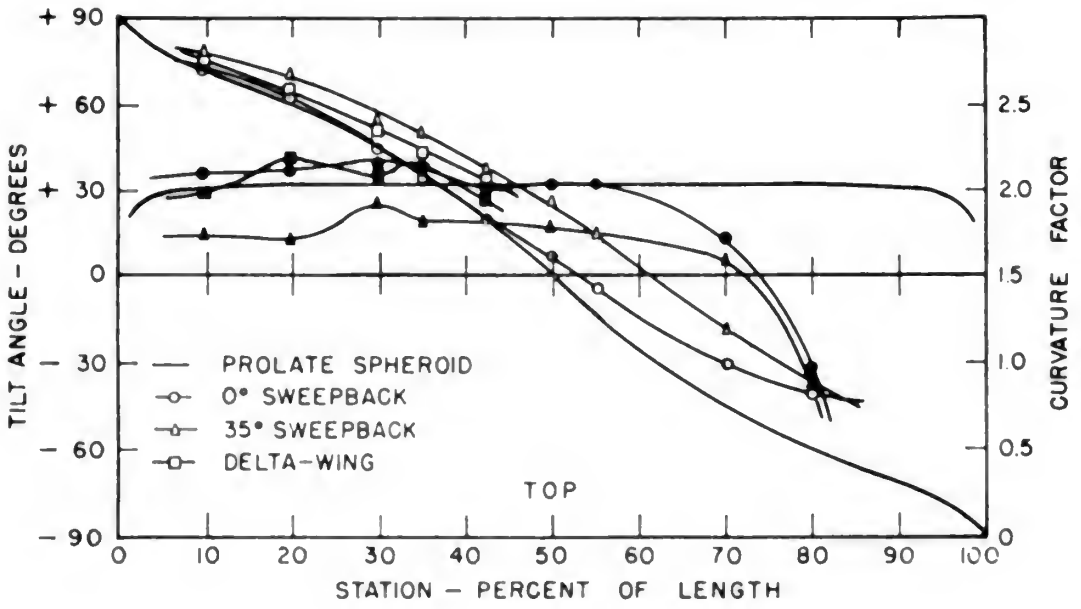

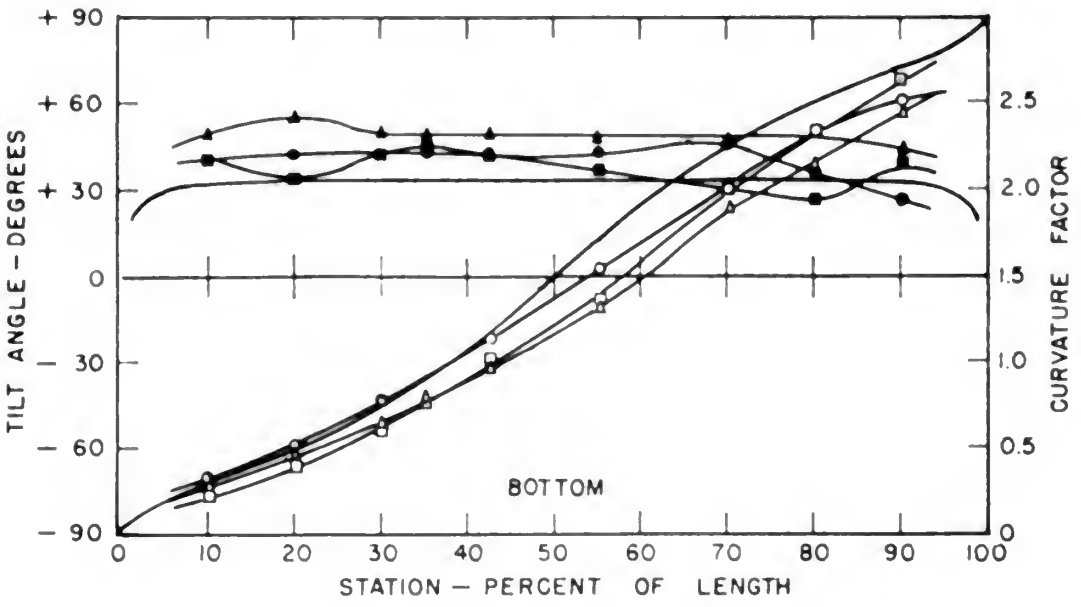

FIG. 23

EFFECT OF SWEEPBACK AT MIDWING POSITION

IA-591-TR38-188

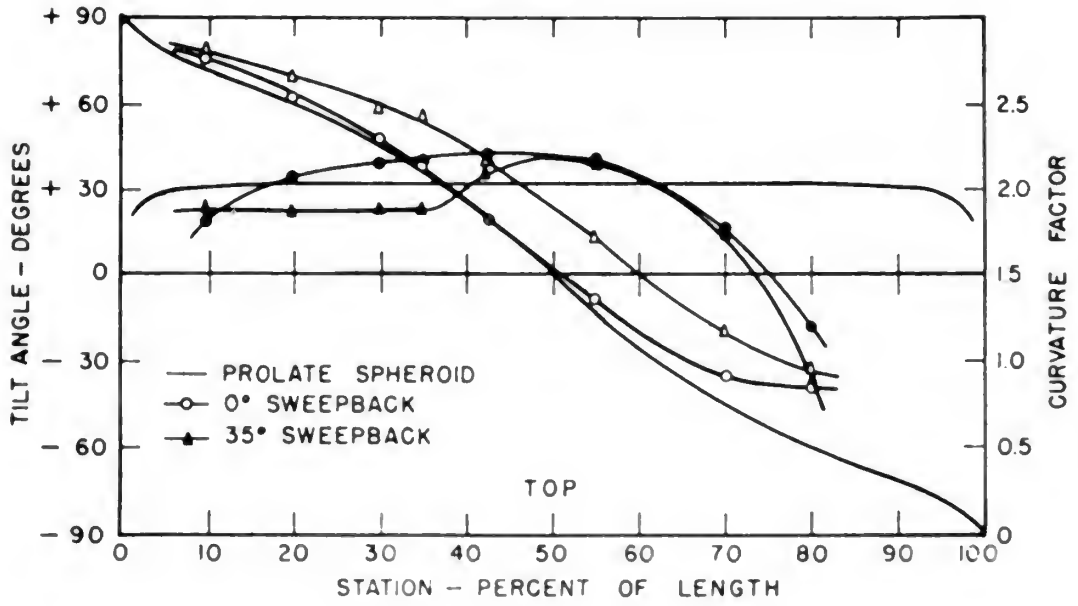

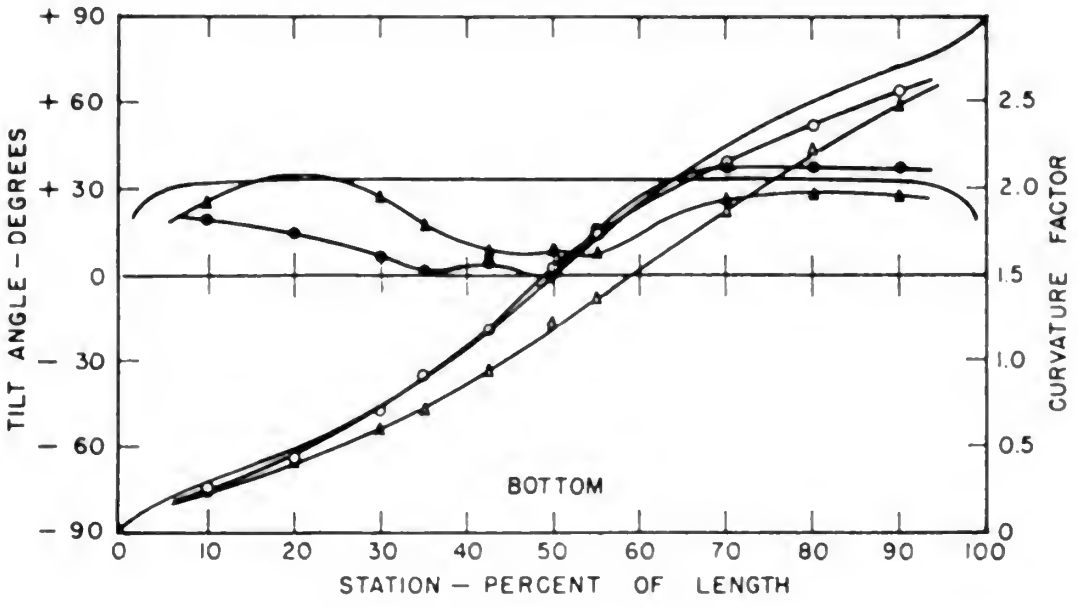

FIG. 24

EFFECT OF SWEEPBACK AT LOW WING POSITION

IA-591-TR38-189

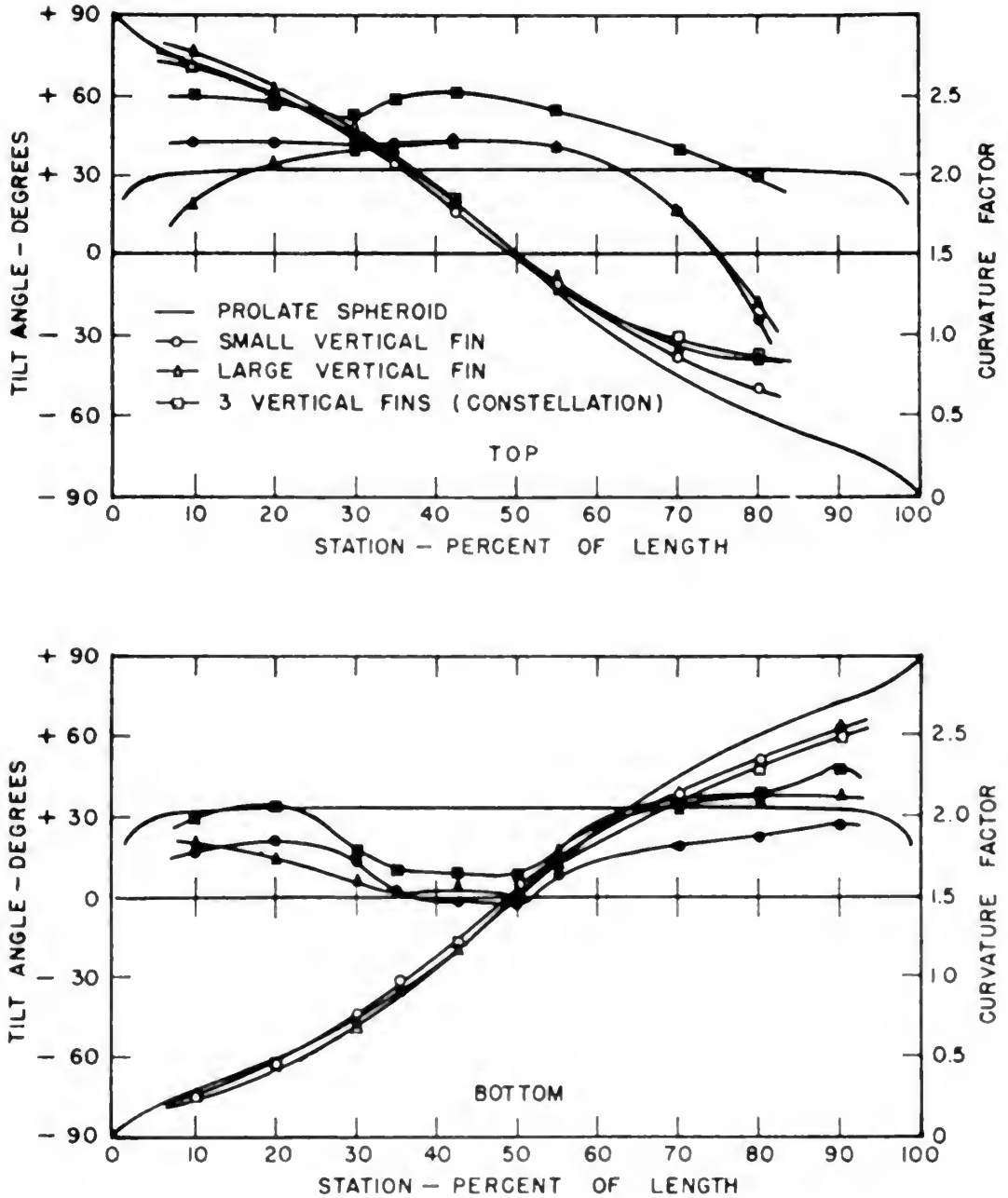

FIG. 25

EFFECT OF VERTICAL FIN CONFIGURATION
AT LOW WING POSITION
(0° SWEEPBACK)

IA-591-TR38-190

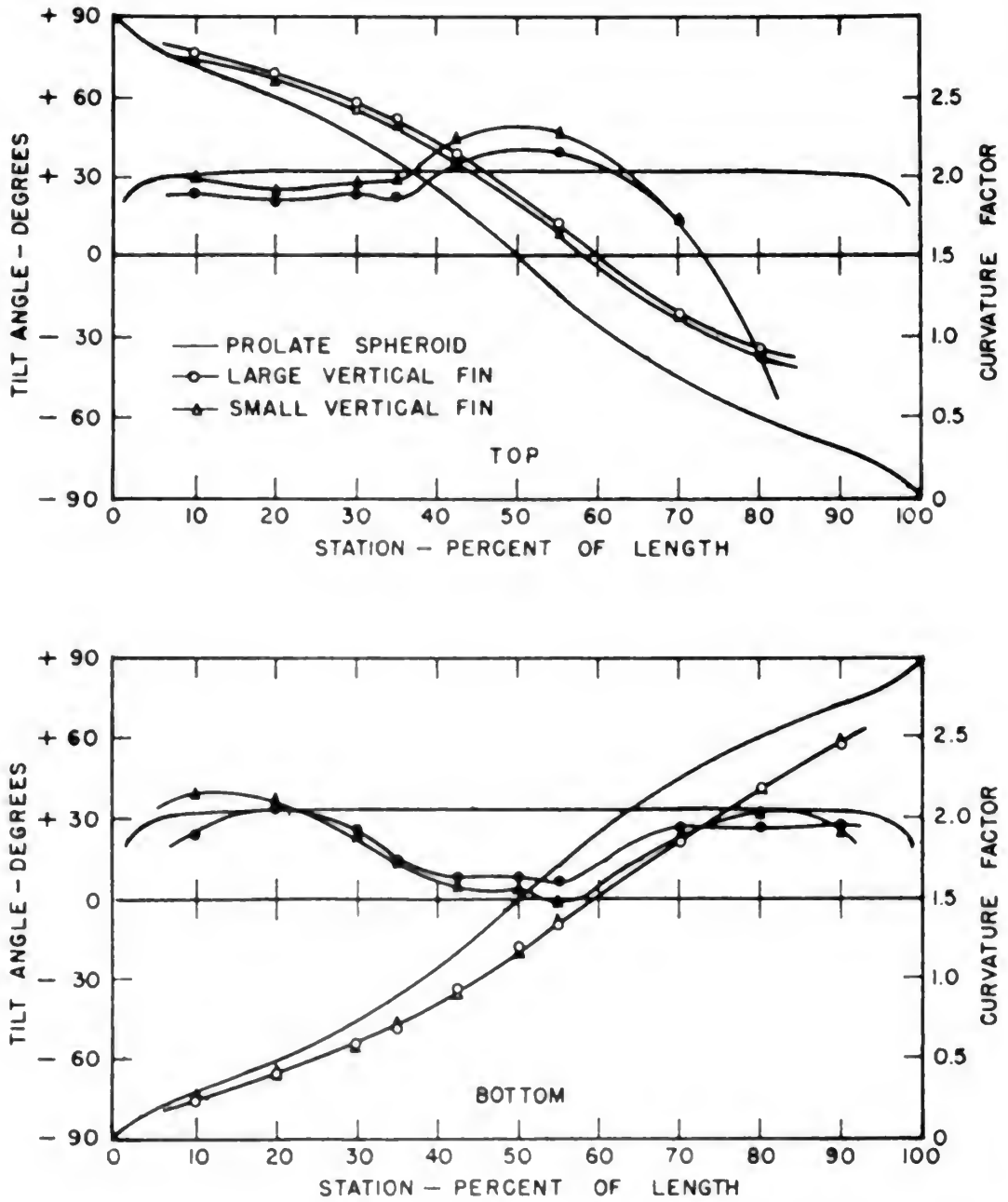

FIG. 26

EFFECT OF VERTICAL FIN CONFIGURATION
AT LOW WING POSITION
(35° SWEEPBACK)

IA-591-TR38-191

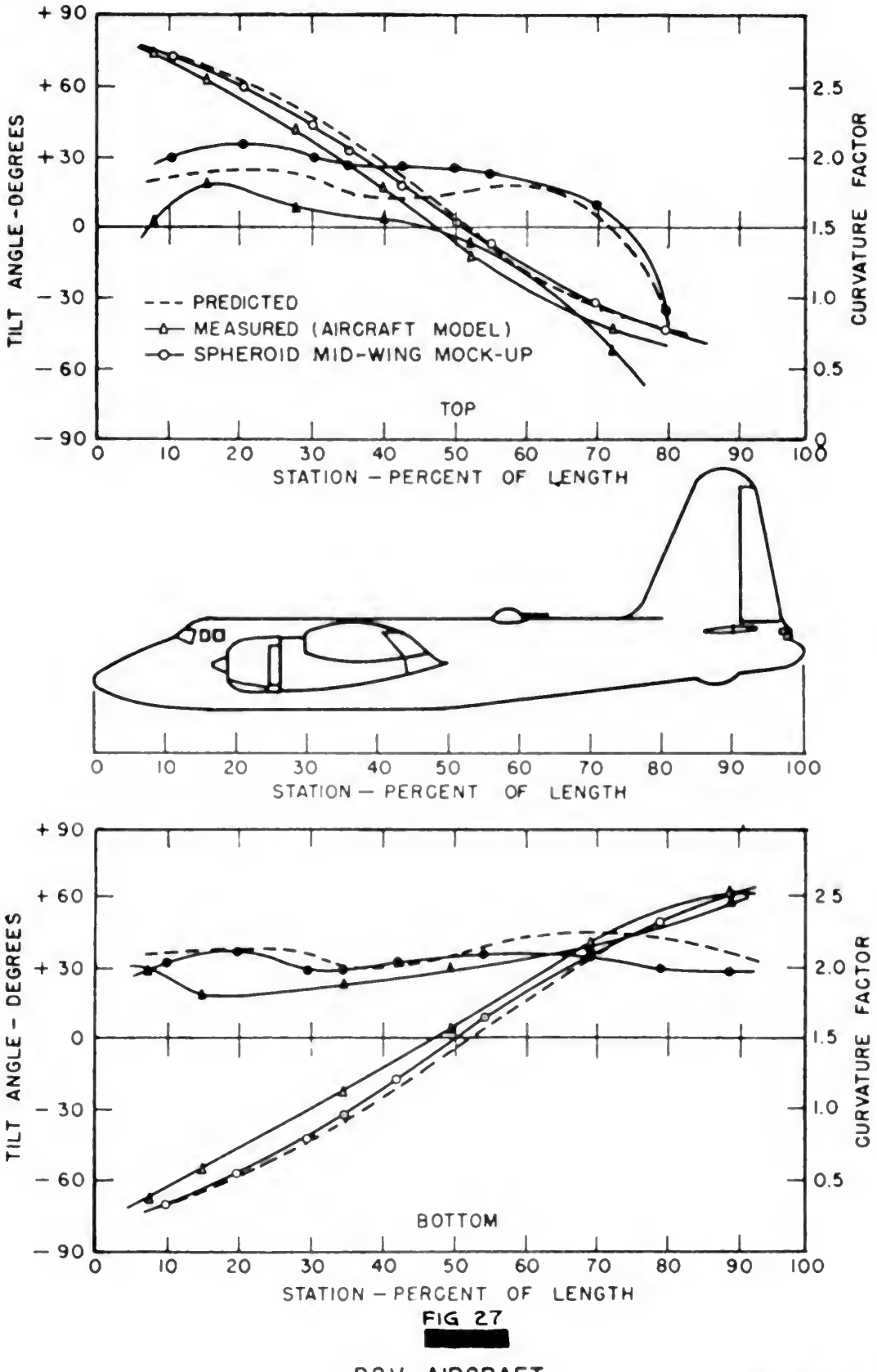

FIG 27

P2V AIRCRAFT

IA-591-TR38-192

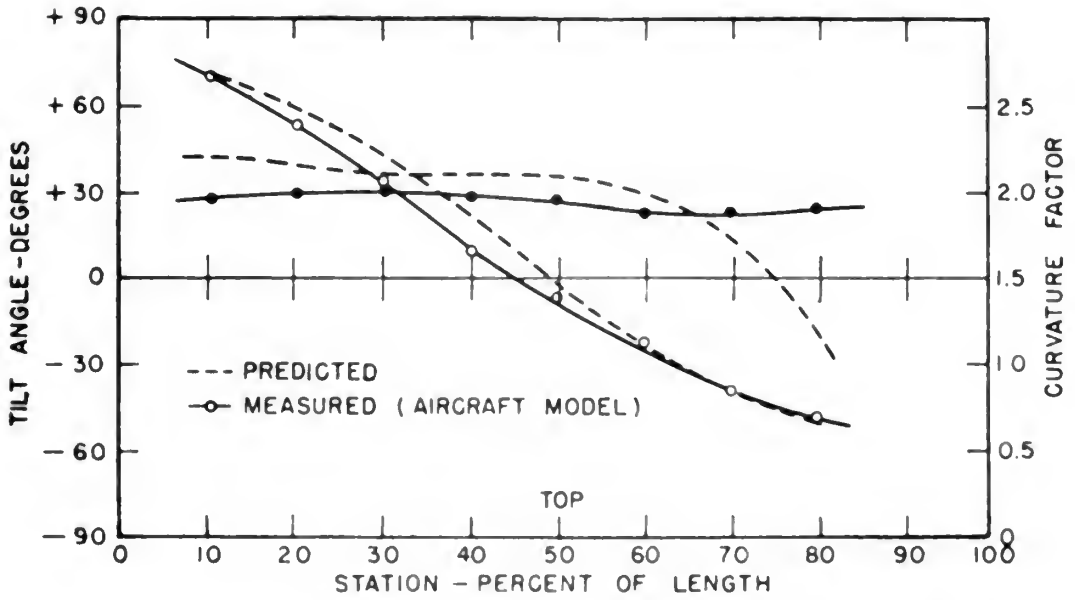

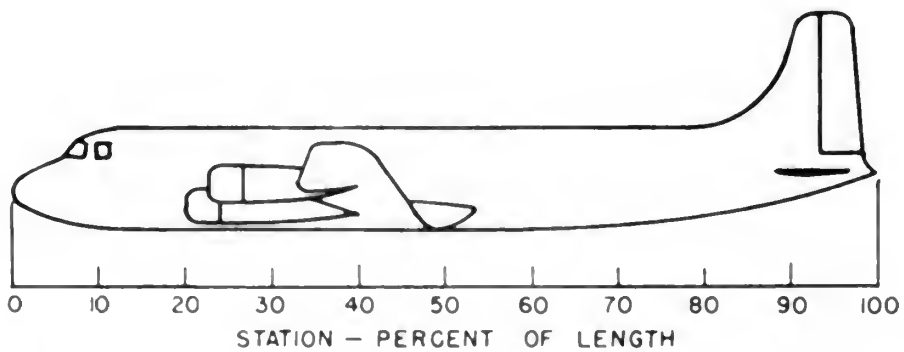

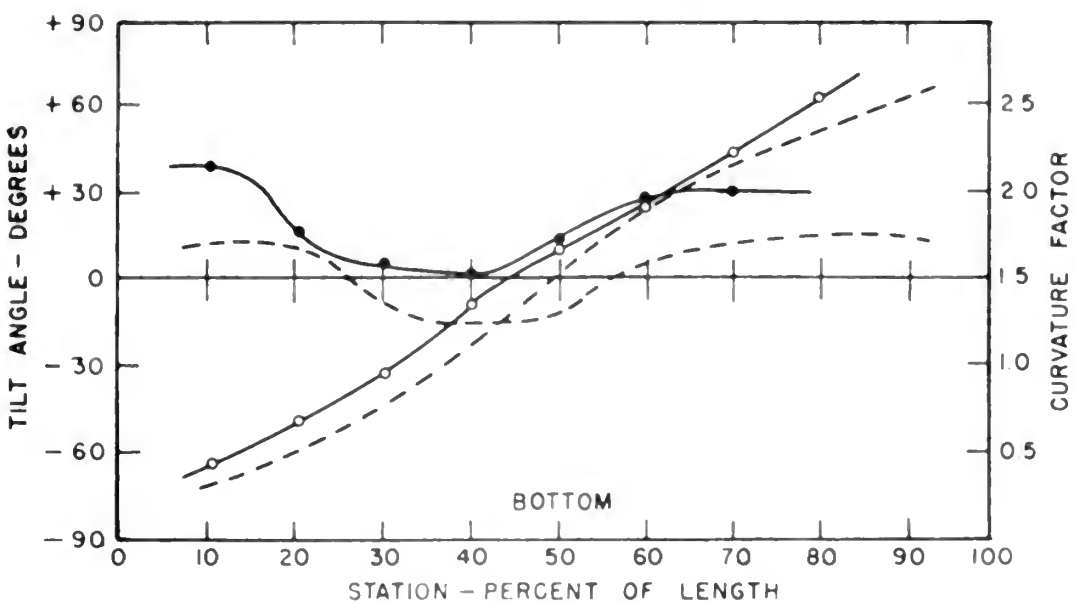

FIG. 28

DC-6 AIRCRAFT

IA-591-TR38-193

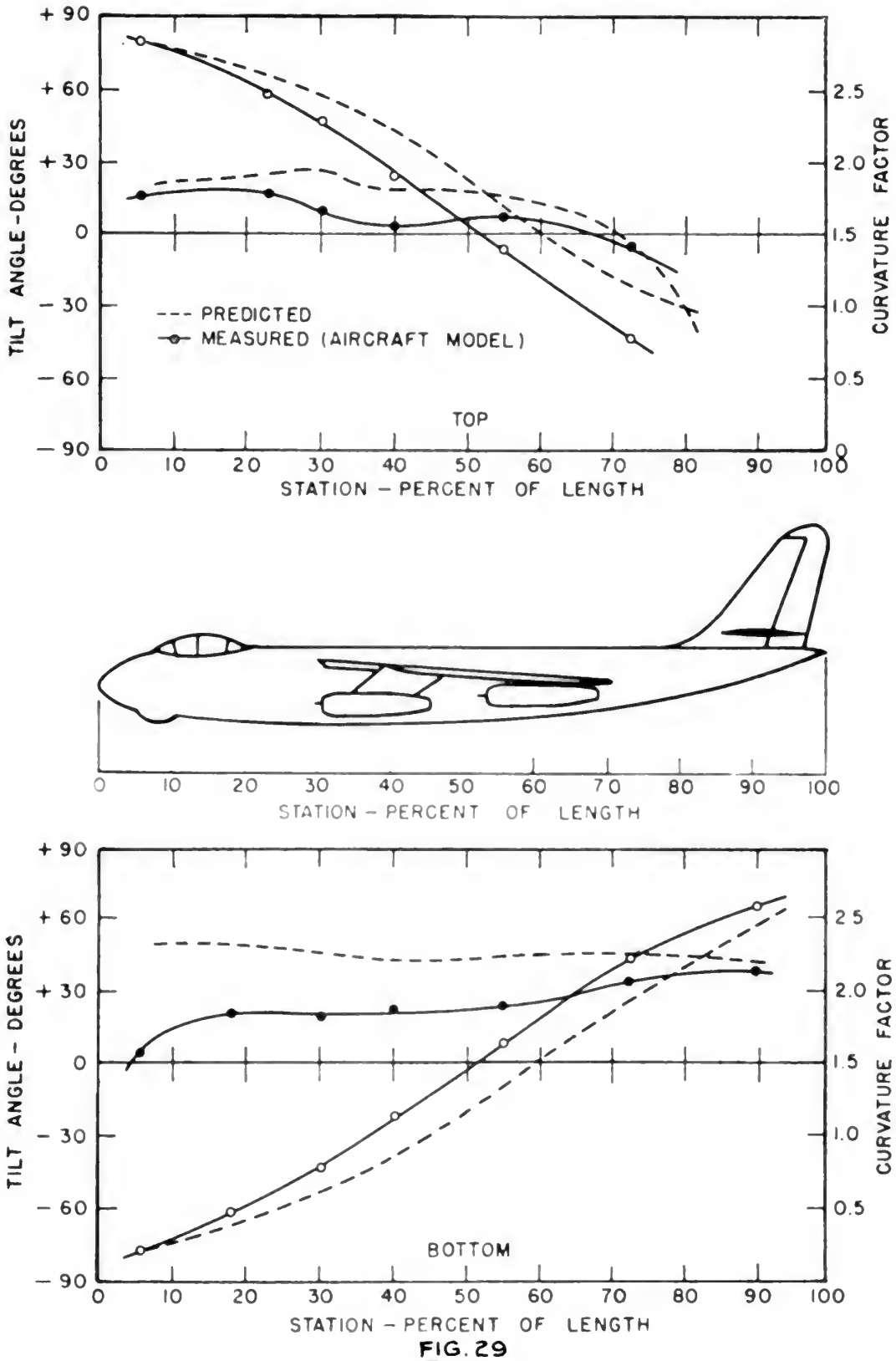

FIG. 29

B-47 AIRCRAFT

IA-591-TR38-194

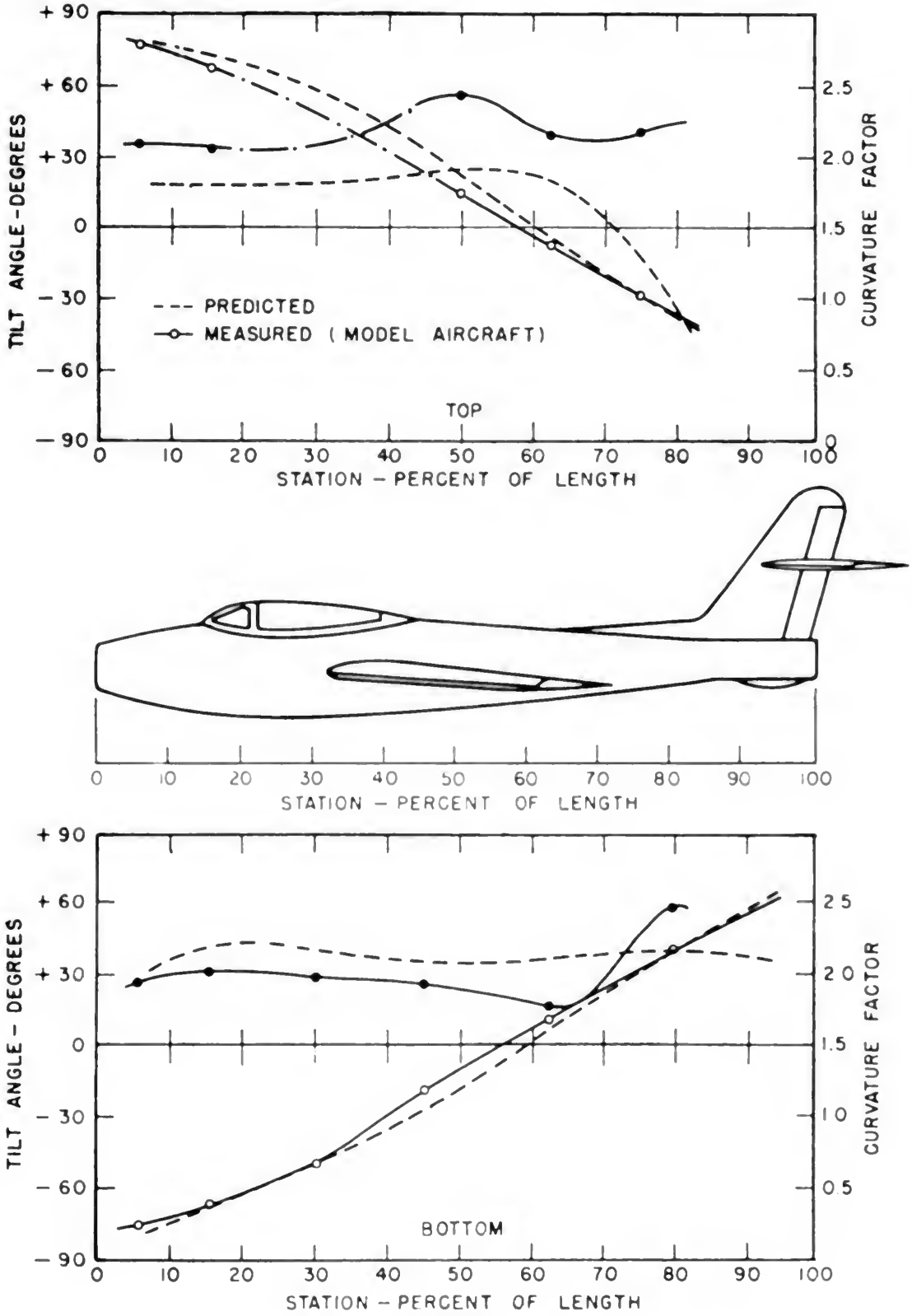

FIG. 30

F-84F AIRCRAFT

IA-591-TR38-195

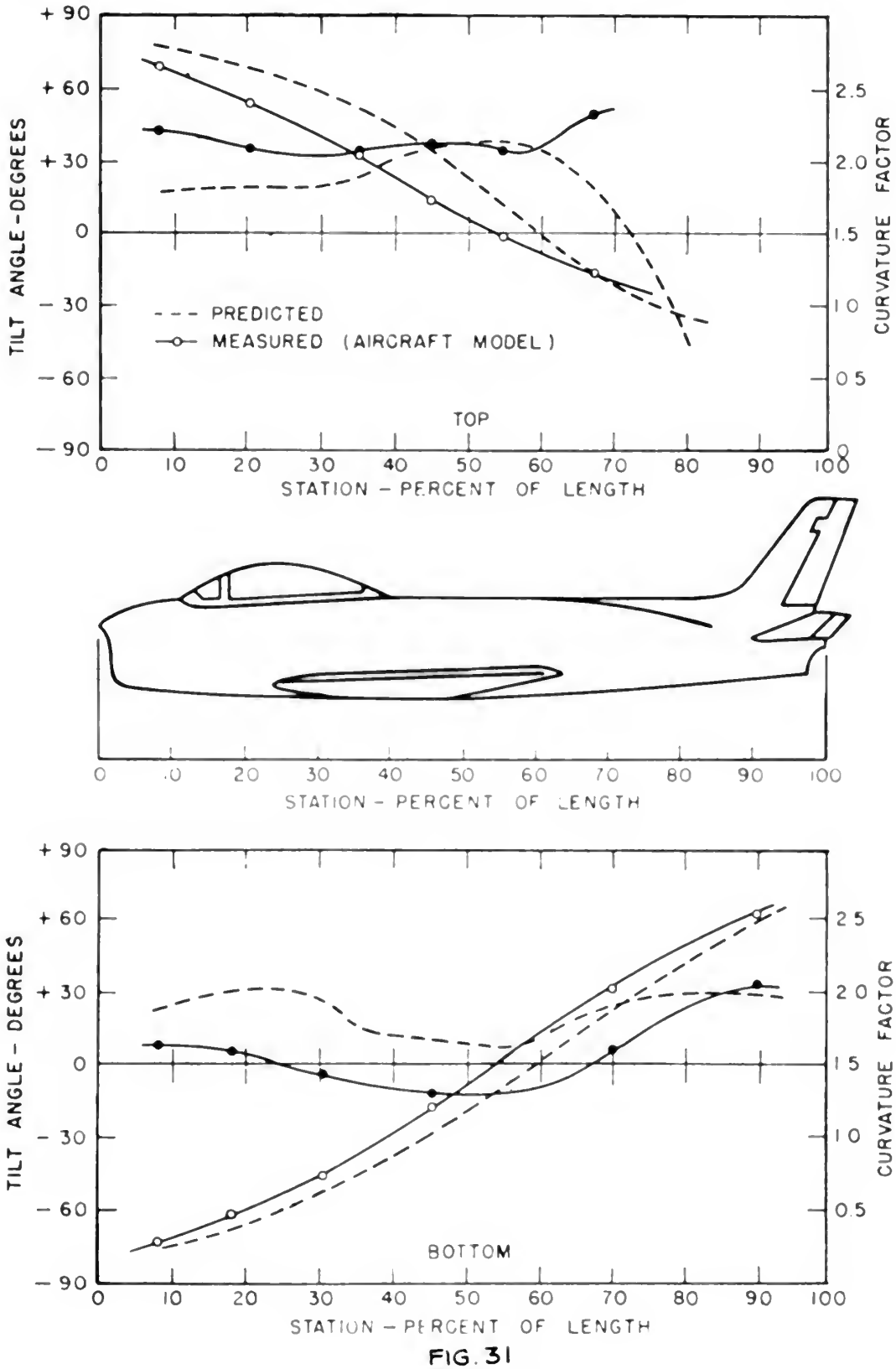

FIG. 31

F-86 AIRCRAFT

IA-591-TR38-196